required for the G(2)/M DNA damage checkpoint. *Genes Dev* **14:** 1448–1459

Lowe SW, Cepero E, Evan G (2004) Intrinsic tumour suppression. *Nature* **432:** 307–315

Maclaine NJ, Hupp TR (2009) The regulation of p53 by phosphorylation: a model for how distinct signals integrate into the p53 pathway. *Aging (Albany NY)* **1:** 490–502

MacLaine NJ, Oster B, Bundgaard B, Fraser JA, Buckner C, Lazo PA, Meek DW, Hollsberg P, Hupp TR (2008) A central role for CK1 in catalyzing phosphorylation of the p53 transactivation domain at serine 20 after HHV-6B viral infection. *J Biol Chem* **283:** 28563–28573

MacPherson D, Kim J, Kim T, Rhee BK, Van Oostrom CT, DiTullio RA, Venere M, Halazonetis TD, Bronson R, De Vries A, Fleming M, Jacks T (2004) Defective apoptosis and B-cell lymphomas in mice with p53 point mutation at Ser 23. *EMBO J* **23:** 3689–3699

Mallette FA, Gaumont-Leclerc MF, Ferbeyre G (2007) The DNA damage signaling pathway is a critical mediator of oncogene-induced senescence. *Genes Dev* **21:** 43–48

Matsuoka S, Huang M, Elledge SJ (1998) Linkage of ATM to cell cycle regulation by the Chk2 protein kinase. *Science* **282:** 1893–1897

McPherson JP, Lemmers B, Hirao A, Hakem A, Abraham J, Migon E, Matysiak-Zablocki E, Tamblyn L, Sanchez-Sweatman O, Khokha R, Squire J, Hande MP, Mak TW, Hakem R (2004) Collaboration of Brca1 and Chk2 in tumorigenesis. *Genes Dev* **18:** 1144–1153

Meijers-Heijboer H, van den Ouweland A, Klijn J, Wasielewski M, de Snoo A, Oldenburg R, Hollestelle A, Houben M, Crepin E, van Veghel-Plandsoen M, Elstrodt F, van Duijn C, Bartels C, Meijers C, Schutte M, McGuffog L, Thompson D, Easton D, Sodha N, Seal S *et al* (2002) Low-penetrance susceptibility to breast cancer due to CHEK2(*)1100delC in noncarriers of BRCA1 or BRCA2 mutations. *Nat Genet* **31:** 55–59

Niida H, Katsuno Y, Banerjee B, Hande MP, Nakanishi M (2007) Specific role of Chk1 phosphorylations in cell survival and checkpoint activation. *Mol Cell Biol* **27:** 2572–2581

Niida H, Tsuge S, Katsuno Y, Konishi A, Takeda N, Nakanishi M (2005) Depletion of Chk1 leads to premature activation of Cdc2-cyclin B and mitotic catastrophe. *J Biol Chem* **280:** 39246–39252

Palmero I, Pantoja C, Serrano M (1998) p19ARF links the tumour suppressor p53 to Ras. *Nature* **395:** 125–126

Sanchez Y, Wong C, Thoma RS, Richman R, Wu Z, Piwnica-Worms H, Elledge SJ (1997) Conservation of the Chk1 checkpoint pathway in mammals: linkage of DNA damage to Cdk regulation through Cdc25. *Science* **277:** 1497–1501

Scheffner M, Werness BA, Huibregtse JM, Levine AJ, Howley PM (1990) The E6 oncoprotein encoded by human papillomavirus types 16 and 18 promotes the degradation of p53. *Cell* **63:** 1129–1136

Serrano M, Lin AW, McCurrach ME, Beach D, Lowe SW (1997) Oncogenic ras provokes premature cell senescence associated with accumulation of p53 and p16INK4a. *Cell* **88:** 593–602

Sharpless NE, Bardeesy N, Lee KH, Carrasco D, Castrillon DH, Aguirre AJ, Wu EA, Horner JW, DePinho RA (2001) Loss of p16Ink4a with retention of p19Arf predisposes mice to tumorigenesis. *Nature* **413:** 86–91

Sherr CJ, DePinho RA (2000) Cellular senescence: mitotic clock or culture shock? *Cell* **102:** 407–410

Shieh SY, Ahn J, Tamai K, Taya Y, Prives C (2000) The human homologs of checkpoint kinases Chk1 and Cds1 (Chk2) phosphorylate p53 at multiple DNA damage-inducible sites. *Genes Dev* **14:** 289–300

Shimada M, Nakanishi M (2008) Checkpoints meet the transcription at a novel histone milestone (H3-T11). *Cell Cycle* **7:** 1555–1559

Shimada M, Niida H, Zineldeen DH, Tagami H, Tanaka M, Saito H, Nakanishi M (2008) Chk1 is a histone H3 threonine 11 kinase that regulates DNA damage-induced transcriptional repression. *Cell* **132:** 221–232

Smits VA, Reaper PM, Jackson SP (2006) Rapid PIKK-dependent release of Chk1 from chromatin promotes the DNA-damage checkpoint response. *Curr Biol* **16:** 150–159

Sorensen CS, Hansen LT, Dziegielewski J, Syljuasen RG, Lundin C, Bartek J, Helleday T (2005) The cell-cycle checkpoint kinase Chk1 is required for mammalian homologous recombination repair. *Nat Cell Biol* **7:** 195–201

Stracker TH, Couto SS, Cordon-Cardo C, Matos T, Petrini JH (2008) Chk2 suppresses the oncogenic potential of DNA replication-associated DNA damage. *Mol Cell* **31:** 21–32

Syljuasen RG, Sorensen CS, Hansen LT, Fugger K, Lundin C, Johansson F, Helleday T, Sehested M, Lukas J, Bartek J (2005) Inhibition of human Chk1 causes increased initiation of DNA replication, phosphorylation of ATR targets, and DNA breakage. *Mol Cell Biol* **25:** 3553–3562

Takai H, Naka K, Okada Y, Watanabe M, Harada N, Saito S, Anderson CW, Appella E, Nakanishi M, Suzuki H, Nagashima K, Sawa H, Ikeda K, Motoyama N (2002) Chk2-deficient mice exhibit radioresistance and defective p53-mediated transcription. *EMBO J* **21:** 5195–5205

Takai H, Tominaga K, Motoyama N, Minamishima YA, Nagahama H, Tsukiyama T, Ikeda K, Nakayama K, Nakanishi M (2000) Aberrant cell cycle checkpoint function and early embryonic death in Chk1(-/-) mice. *Genes Dev* **14:** 1439–1447

Toledo LI, Murga M, Gutierrez-Martinez P, Soria R, Fernandez-Capetillo O (2008) ATR signaling can drive cells into senescence in the absence of DNA breaks. *Genes Dev* **22:** 297–302

Tominaga K, Morisaki H, Kaneko Y, Fujimoto A, Tanaka T, Ohtsubo M, Hirai M, Okayama H, Ikeda K, Nakanishi M (1999) Role of human Cds1 (Chk2) kinase in DNA damage checkpoint and its regulation by p53. *J Biol Chem* **274:** 31463–31467

Vahteristo P, Bartkova J, Eerola H, Syrjakoski K, Ojala S, Kilpivaara O, Tamminen A, Kononen J, Aittomaki K, Heikkila P, Holli K, Blomqvist C, Bartek J, Kallioniemi OP, Nevanlinna H (2002) A CHEK2 genetic variant contributing to a substantial fraction of familial breast cancer. *Am J Hum Genet* **71:** 432–438

Varmark H, Kwak S, Theurkauf WE (2010) A role for Chk2 in DNA damage induced mitotic delays in human colorectal cancer cells. *Cell Cycle* **9:** 312–320

Yu Q, Rose JH, Zhang H, Pommier Y (2001) Antisense inhibition of Chk2/hCds1 expression attenuates DNA damage-induced S and G2 checkpoints and enhances apoptotic activity in HEK-293 cells. *FEBS Lett* **505:** 7–12

Zaugg K, Su YW, Reilly PT, Moolani Y, Cheung CC, Hakem R, Hirao A, Liu Q, Elledge SJ, Mak TW (2007) Cross-talk between Chk1 and Chk2 in double-mutant thymocytes. *Proc Natl Acad Sci USA* **104:** 3805–3810

Essential role of Tip60-dependent recruitment of ribonucleotide reductase at DNA damage sites in DNA repair during G1 phase

Hiroyuki Niida,[1] Yuko Katsuno,[1] Misuzu Sengoku,[1] Midori Shimada,[1] Megumi Yukawa,[1] Masae Ikura,[2] Tsuyoshi Ikura,[2] Kazuteru Kohno,[3] Hiroki Shima,[3] Hidekazu Suzuki,[3] Satoshi Tashiro,[3] and Makoto Nakanishi[1,4]

[1]Department of Cell Biology, Graduate School of Medical Sciences, Nagoya City University Medical School, Nagoya 467-8601, Japan; [2]Radiation Biology Center, Kyoto University, Kyoto 606-8501, Japan; [3]Department of Cell Biology, Research Institute for Radiation Biology and Medicine (RIRBM), Hiroshima University, Hiroshima 734-8553, Japan

A balanced deoxyribonucleotide (dNTP) supply is essential for DNA repair. Here, we found that ribonucleotide reductase (RNR) subunits RRM1 and RRM2 accumulated very rapidly at damage sites. RRM1 bound physically to Tip60. Chromatin immunoprecipitation analyses of cells with an I-SceI cassette revealed that RRM1 bound to a damage site in a Tip60-dependent manner. Active RRM1 mutants lacking Tip60 binding failed to rescue an impaired DNA repair in RRM1-depleted G1-phase cells. Inhibition of RNR recruitment by an RRM1 C-terminal fragment sensitized cells to DNA damage. We propose that Tip60-dependent recruitment of RNR plays an essential role in dNTP supply for DNA repair.

Supplemental material is available at http://www.genesdev.org.

Received September 15, 2009; revised version accepted December 22, 2009.

Maintenance of the optimal intracellular concentrations of deoxyribonucleotides (dNTPs) is critical not only for faithful DNA synthesis during DNA replication and repair, but also for the survival of all organisms. Ribonucleotide reductase (RNR), composed of a tetrameric complex of two large catalytic (RRM1) subunits and two small subunits (RRM2 or 53R2), catalyzes de novo synthesis of dNTPs from the corresponding ribonucleotides (Reichard 1993). This reaction is the rate-limiting process in DNA precursor synthesis and is regulated by multiple complex mechanisms, including transcriptional and subcellular localization regulation of RNR (Nordlund and Reichard 2006). In order to duplicate their chromosomal DNA, mammalian S-phase cells possess 15–20 times more dNTP pools than resting quiescent cells, whereas whole dNTP pools were almost unchanged after DNA damage, suggesting the presence of a unique mechanism that supplies a sufficient quantity of dNTPs at repair sites (Hakansson et al. 2006). DNA synthesis must function properly in both repair and replication (dNTP concentrations in fibroblasts were estimated to be as follows: ~0.5 μM in G0/G1-phase cells, and ~10 μM in S-phase cells, given that the average volume of a fibroblast is 3.4 pL) (Imaizumi et al. 1996). Although the amount of dNTPs required for DNA repair is small, their concentration during DNA synthesis is critical because DNA polymerase involved in DNA repair (Kraynov et al. 2000; Johnson et al. 2003) has similar kinetic affinities for dNTPs (~10 μM) to those involved in DNA replication (~10 μM) (Dong and Wang 1995). Therefore, the dNTPs might be compartmentalized close to the damage sites during the DNA repair process. In this study, we show that, in mammals, both RRM1 and RRM2 rapidly accumulated at double-strand break (DSB) sites in a Tip60-binding-dependent manner.

[*Keywords*: DNA repair; ribonucleotide reductase; Tip60; dNTPs; genomic instability; DNA double-strand breaks]
[4]**Corresponding author.**
E-MAIL mkt-naka@med.nagoya-cu.ac.jp, FAX 81-52-842-3955.
Article is online at http://www.genesdev.org/cgi/doi/10.1101/gad.1863810.

Results and Discussion

In order to understand the mechanisms by which dNTPs are sufficiently supplied at DNA damage sites in mammals, we first examined changes in the subcellular localization of RRM1 and RRM2 subunits after ionizing irradiation (IR) irradiation. Although both RRM1 and RRM2 predominantly localized in the cytoplasm as reported previously (Pontarin et al. 2008), we also detected trace, but significant, signals of both proteins in chromatin fraction (see Fig. 1C; Supplemental Fig. S4A–D). After removing soluble RNR proteins by detergent extraction, we found that RRM1 and RRM2 proteins formed nuclear foci that colocalized with γH2AX (Fig. 1A). RRM1 nuclear foci were not evident without DNA damage (Supplemental Fig. S1A) or after RRM1 depletion by siRNA (Supplemental Fig. S1B). Ultravioulet A (UVA) microirradiation resulted in the accumulation of RRM1 and RRM2 along microirradiated lines as early as 5 min after treatment (Fig. 1B). These accumulations were also observed when cells were not subjected to detergent extraction or preincubation with BrdU (Supplemental Fig. S2A,B), but were significantly compromised when R1 expression was knockdown by siRNA (Supplemental Figs. S2C, S4B), excluding the possibility that accumulated signals at DSB sites were artifacts during cell-staining processes. These results indicated that RNR, at least in part, was rapidly recruited to DSB sites.

In order to determine the molecular basis underlying RNR recruitment at the sites of DSBs, we performed yeast two-hybrid screening using RRM1 as a bait. Of a total of 5×10^6 transformants from a HeLa cell cDNA library, 45 positive colonies were confirmed to be lacZ-positive. They contained overlapping cDNAs derived from three genes: *RRM2* and *53R2* (both encoding a small subunit of RNR), and another encoding *Tip60* histone acetyltransferase (Tip60). Small C-terminal RRM1 deletion mutants (Δ761-C and Δ781-C) failed to bind Tip60, but retained the ability to bind to RRM2 (Supplemental Fig. S3A). In contrast, the N-terminal truncation mutant of Tip60

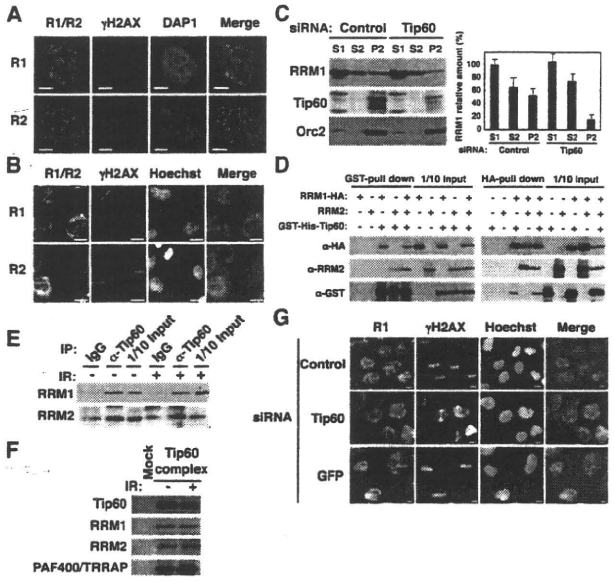

Figure 1. Tip60-dependent recruitment of RNR at DSB sites. (*A*) HeLa cells were exposed to IR at 1 Gy, subjected to in situ detergent extraction after 5 min, and immunostained with the indicated antibodies. Bars, 5 μm. (*B*) GM02063 cells were subjected to UVA microirradiation and immunostained with the indicated antibodies after 5 min. RRM1 or RRM2 and γH2AX signals are shown in green and red, respectively, in merged images. Bars, 10 μm. (*C*) IR-irradiated HeLa cell lysates treated with the indicated siRNAs were fractionated as described in the Materials and Methods. (*Left* panels) The fractions were subjected to immunoblotting using the indicated antibodies. (*Right* panel) The RRM1 bands were quantitated, and the results are presented as percentages of S1 fraction. Data are mean ± standard deviation (n = 3). (*D*) Sf9 lysates expressing RRM1-HA, RRM2, or GST-His-Tip60 were subjected to GST pull-down or HA pull-down assays using the indicated antibodies. (*E*) Chromatin fractions from IR- or mock-treated HeLa cells (after 5 min) were solubilized with micrococcal nuclease. The solubilized extracts were immunoprecipitated with anti-Tip60 antibodies or control IgG. The resulting precipitates and a 10% input (1/10 Input) were immunoblotted with the indicated antibodies. (*F*) The affinity-purified Tip60 complexes, as described in the Materials and Methods, were subjected to immunoblotting using the indicated antibodies. (*G*) GM02063 cells were treated with control, Tip60, or GFP siRNAs and then subjected to UVA microirradiation as in *B*.

(TC2) could interact with RRM1, but no mutant with any additional truncation of TC2 was able to do so (Supplemental Fig. S3B). Full-length Tip60 failed to bind full-length RRM2 (Supplemental Fig. S3C). We generated the C-terminal fragment of RRM1 (amino acids 701–792) with a SV40 nuclear localization signal (NLS-RC1-HA) and examined its ability to bind Tip60 in vivo and in vitro. NLS-RC1-HA, but not a control NL-GFP-HA fragment, was detected in the anti-Myc immunoprecipitates when transiently coexpressed with Tip60-Myc (Supplemental Fig. S3D). Purified MBP-fused RC1 produced in *Escherichia coli* was capable of binding to GST-Tip60 expressed in insect cells (Supplemental Fig. S3E). Both Δ761-C and Δ781-C failed to bind chromatin, further confirming that the binding of RRM1 to chromatin required its interaction with Tip60 (Supplemental Fig. S3F).

Similarly to Chk1 (Niida et al. 2007; Shimada et al. 2008), endogenous RRM1 was present in cytosolic (S1), nucleoplasmic (S2), and chromatin-bound (P2) fractions (Supplemental Fig. S4A). Tip60 existed predominantly in the chromatin-bound fraction (P2). Both RRM1 and Tip60 proteins in this fraction were partly solubilized by treatment with micrococcal nuclease (Mnase), suggesting that they associated with chromatin. RRM1 knockdown showed a significant decrease of RRM1 protein levels in both soluble and chromatin-bound fractions (Supplemental Fig. S4B). IKKα and Orc2 were detected predominantly in soluble and chromatin fractions, respectively, indicating that cell fractionation was done successfully. Ectopic RRM1-HA present in the chromatin fraction was increased when Tip60-Myc-His was coexpressed, although a low level of RRM1-HA was detected in the absence of Tip60-Myc-His, presumably due to the presence of endogenous Tip60 (Supplemental Fig. S4C). The amounts of RRM1 and Tip60 bound to the chromatin were not affected by DNA damage (Supplemental Fig. S4D). However, depletion of Tip60 resulted in a reduction in the amount of RRM1 on chromatin (Fig. 1C). Taken together, chromatin binding of RRM1 appeared to be Tip60-dependent. RRM1-HA, but not the RRM2 subunit alone, formed a complex with GST-His-Tip60 in insect cells (Fig. 1D, left panels). RRM2 also formed a complex with GST-His-Tip60 in a manner dependent on the presence of RRM1-HA. Consistently, accumulation of RRM2 at DSB sites was compromised when RRM1 was depleted (Supplemental Fig. S2D). Immunoprecipitations using anti-HA antibodies demonstrated that RRM1-HA bound to both RRM2 and GST-His-Tip60 (Fig. 1D, right panels). RRM1 and RRM2 were detected in the precipitates of anti-Tip60 antibodies from the solubilized chromatin, even in the absence of DNA damage (Fig. 1E). To further confirm the interaction between RNR and Tip60, we purified the Tip60 complex from HeLa cell nuclear extracts expressing Flag-HA Tip60 as reported previously (Ikura et al. 2000, 2007). RRM1 and RRM2, as well as PAF400/TRRAP as a positive control (Murr et al. 2006), were detected in Tip60 complex from extracts with or without DNA damage (Fig. 1F). Tip60 knockdown by siRNA or shRNA abrogated accumulation of RRM1 along with microirradiated lines (Fig. 1G; Supplemental Fig. S2E). These results suggested that RRM1 recruitment at DSB sites was Tip60-dependent.

To determine precisely whether RRM1 was recruited at the site of DNA damage, we generated *Ku*-deficient mouse embryonic fibroblasts (MEFs) in which a single DSB was introduced after infection with adenoviruses expressing I-SceI. This DSB was not rapidly repaired by nonhomologous end-joining, making it easy to detect proteins accumulating at this DSB site by chromatin immunoprecipitation (ChIP) analysis (*STEFKu70*$^{-/-}$*phprt-DR-GFP*) (Fig. 2A; Pierce et al. 2001). Introduction of the DSB was confirmed by Southern blotting (Supplemental Fig. S5). ChIP analyses revealed a substantial increase in the binding of RRM1 as well as Rad51 and Tip60 to a DNA break site. An increase in acetylation of histone H4 was also observed at the damage site (Fig. 2B). These were not seen on infection with control LacZ. Tip60 depletion by two independent siRNAs resulted in a loss of RRM1 binding to a DSB site, as well as a reduction in acetylation of histone H4 (Fig. 2C). A mutant Tip60 lacking histone-acetylating activity could recruit RRM1 to the DSB site similarly to wild-type RRM1 (Supplemental Fig. S6A). Inhibition of ATM, ATR, and DNA-PK by caffeine did not affect RRM1 recruitment (Supplemental Fig. S6B). These results further supported the notion that complex

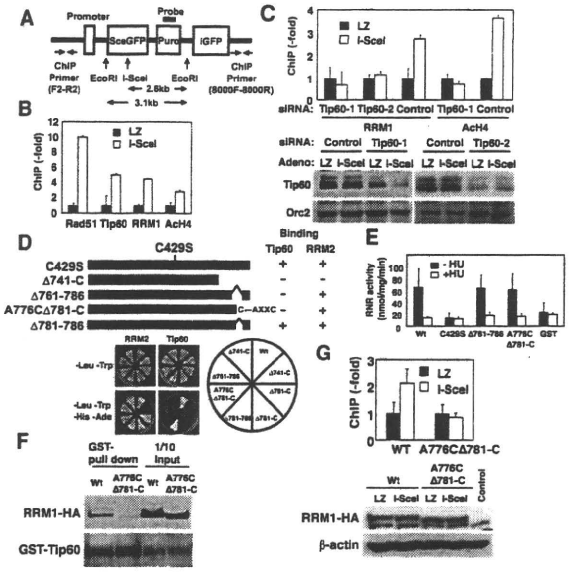

Figure 2. RRM1 is recruited at DSB sites in a Tip60-dependent manner. (*A*) Map of the I-SceI cassette construct containing the I-SceI site, the probe for Southern blotting, and a set of primers for the ChIP assay. (*B*) *STEFKu70*$^{-/-}$*phprt-DR-GFP* cells infected with I-SceI adenoviruses were subjected to ChIP analysis using the indicated antibodies as described in the supporting Materials and Methods. Data are shown as percentages of increases in PCR products from cells expressing I-SceI (I-SceI) relative to those from cells expressing Lac Z (LZ). Data are mean ± standard deviation (n = 3). (*C*) *STEFKu70*$^{-/-}$*phprt-DR-GFP* cells were transfected with two independent Tip60 siRNAs (Tip60-1 and Tip60-2) or control siRNA. ChIP analysis was performed as in *B*. (*Bottom* panels) Aliquots of cell lysates were subjected to immunoblotting using anti-Tip60 antibodies. (*D*) The constructs used are schematically represented, and the specific interaction between RRM1 mutants and Tip60 was assayed using yeast two-hybrid screening. (*E*) An in vitro RNR assay of complexes containing wild-type or various RRM1 mutants was performed as described in the Materials and Methods. (Black bars) −HU; (white bars) +HU (10 mM). Data are mean ± standard deviation (n = 3). (*F*) Sf9 lysates expressing GST-His-Tip60 and the indicated RRM1-HA were subjected to GST pull-down assay using the indicated antibodies. (*G*) Knockout-knock-in *STEFKu70*$^{-/-}$*phprt-DR-GFP* cells expressing wild-type or A776CΔ781-C RRM1-HA were generated by transfection with vectors for either wild-type or A776CΔ781-C RRM1 and then with RRM1 siRNA. Expression vectors of wild type and A776CΔ781-C contain mutations in a specific sequence targeted by siRNA. (*Top* panel) Cells were subjected to ChIP analysis using anti-HA antibodies as in *B*. (*Bottom* panels) Aliquots of cell lysates were subjected to immunoblotting using the indicated antibodies.

formation between RNR and Tip60 is required for recruitment of RNR to sites of DNA damage.

We then examined if RNR recruitment at damage sites was required for effective DNA repair. We first generated RRM1 mutants that lack the ability to bind Tip60 but retain RNR activity. Given that the C-terminal CXXC motif of RRM1 is important for RNR function (Zhang et al. 2007), we constructed *RRM1* mutants containing the CXXC motif but lacking Tip60-binding ability (Δ761–786 and A776CΔ781-C) (Fig. 2D). Wild-type RRM1 or its mutants were coexpressed with RRM2 in insect cells, and the resultant complexes were subjected to an in vitro RNR assay (Fukushima et al. 2001). RNR complexes containing wild-type, Δ761–786, and A776CΔ781-C RRM1 retained hydroxyurea (HU)-sensitive RNR activity (HU is a specific RNR inhibitor), whereas an inactive C429S mutant or GST protein as a negative control did not show RNR activity (Fig. 2E). The specific activity of RNR containing wild-type, Δ761–787, and A776CΔ781-C RRM1 (~50 nmol/mg per minute) was similar to that reported previously (Guittet et al. 2001), confirming the reliability of our results. The A776CΔ781-C mutant failed to form a complex with GST-Tip60 (Fig. 2F). ChIP analysis using RRM1 knockout–knock-in *STEFKu70*$^{-/-}$*phprt-DR-GFP* cells revealed that the A776CΔ781-C mutant failed to accumulate at the DSB site (Fig. 2G). These results indicated that direct interaction of RRM1 to Tip60 is required for triggering its accumulation at the DSB site.

A comet assay revealed that DNA damage in cells was repaired efficiently within 1 h in the absence of HU. However, treatment with HU, and RRM1 or RRM2 depletion, resulted in an impairment of DNA repair (Fig. 3A,B). RNR activity was thus essential for effective repair. Ectopic expression of wild-type *RRM1* with mutations in a specific sequence targeted by siRNA effectively rescued the impaired DNA repair in cells depleted of endogenous RRM1 (Fig. 3C). In contrast, ectopic expression of C429S, Δ761–786, and A776CΔ781-C RRM1 failed

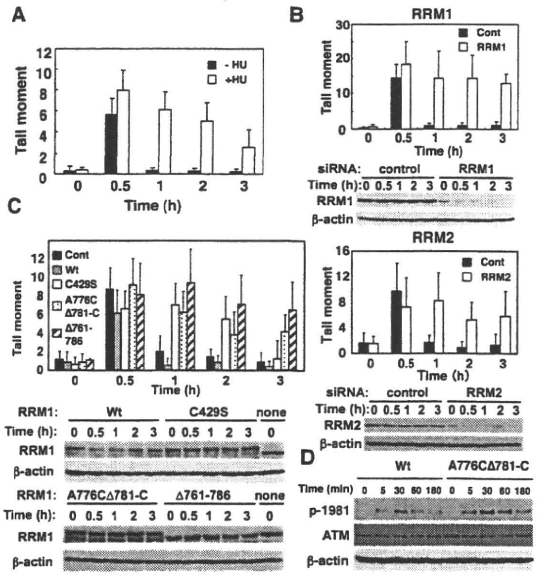

Figure 3. Recruitment of active RNR at DNA damage sites is a prerequisite for effective DNA repair. (*A*) HeLa cells were treated with (open bars) or without (filled bars) 2.5 mM HU, exposed to IR (4 Gy), and subjected to a comet assay as described in the Materials and Methods. The results were obtained by counting at least 50 cells per sample in three independent experiments. (*B*) HeLa cells were transfected with a control (filled bars) or RRM1 or RRM2 siRNA (open bars), and DNA repair was evaluated as in *A*. Cell lysates were subjected to immunoblotting using the indicated antibodies. (*C*) HeLa cells were transfected with or without (filled bars) either wild-type (gray bars), C429S (open bars), A776CΔ781-C (dotted), or Δ761–786 (hatched) RRM1. RRM1-transfected cells were then transfected with RRM1 siRNA. Expression vectors of wild type and various RRM1 mutants contain mutations in a specific sequence targeted by siRNA. DNA repair activity and expression of RRM1 were examined as in *B*. (*D*) Knockout–knock-in HeLa cells expressing wild type or A776CΔ781-C RRM1-HA were exposed to IR, and cell lysates were subjected to immunoblotting as in *C*.

to do so. ATM was activated independently of Tip60 binding to RNR, but this activation was enhanced and prolonged in cells expressing A776CΔ781-C, presumably due to impaired DNA repair (Fig. 3D). It is therefore conceivable that recruitment of active RNR at DNA damage sites is a prerequisite for effective DSB repair, but not for activation of checkpoint signaling. Tip60 is also known to participate in transcriptional regulation of several genes. Neither RRM1 nor RRM2 proteins were affected by Tip60 depletion or overexpression (Supplemental Fig. S7), indicating that the effect of Tip60 did not result from changes in RRM1 and RRM2 expression.

ChIP analyses revealed that NLS-RC1-HA specifically inhibited RRM1 binding, but did not affect Rad51 or Tip60 binding, or increase H4 acetylation at the DSB site in *STEFKu70*$^{-/-}$*phprt-DR-GFP* cells (Fig. 4A). Expression of NLS-RC1-HA suppressed accumulation of endogenous RRM1 at DNA damage sites (Supplemental Fig. S8A,B), but did not affect the foci formation of 53BP1 at DSB sites (Fig. 4B), or complex formation and activity (Supplemental Fig. S9A,B) of endogenous RNR. However, cells expressing NLS-RC1-HA, but not NLS-GFP-HA, had unrepaired DNA in the tail at 2 h (Fig. 4C). A quantitative colony formation assay was used to examine the DNA damage sensitivity of cells expressing NLS-RC1-HA. Induction of NLS-RC1-HA sensitized cells to IR (Fig. 4D).

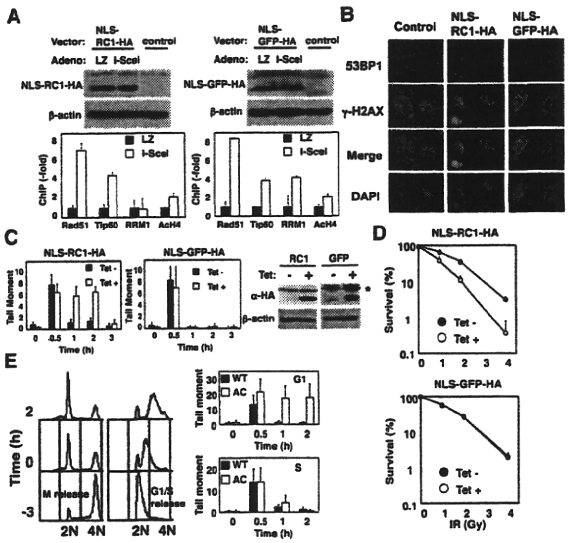

Figure 4. Inhibition of recruitment of RNR at DSB sites by ectopic expression of NLS-RC1-HA abrogates DNA repair and sensitizes cells to DNA damage. (*A*) *STEFKu70*$^{-/-}$*phprt-DR-GFP* cells expressing NLS-RC1-HA (SV40 NLS-RC1 fragment, 701–792 amino acids) or NLS-GFP-HA (GFP fragment, 1–93 amino acids) were subjected to ChIP analysis as in Figure 2B. (*Top* panels) Cell lysates were subjected to immunoblotting using the indicated antibodies. (*B*, *left* panels) Tet-on HeLa cells expressing NLS-RC1-HA or NLS-GFP-HA were treated with or without tetracycline (1 μg/mL), exposed to IR (4 Gy), and subjected to immunostaining with the indicated antibodies and a comet assay as in Figure 3A. (*Right* panels) IR-untreated lysates were subjected to immunoblotting using the indicated antibodies. (*C*) Asterisk (*) represents nonspecific bands. (*D*) These cells were exposed to the indicated dose of IR, and a quantitative colony formation assay was performed 8 d after treatment. Data are mean ± standard deviation (n = 3). (*E*) Knockout–knock-in HeLa cells expressing either wild-type (filled bars) or A776CΔ781-C (open bars) RRM1-HA were synchronized as described in the Materials and Methods. Synchronized cells were then released into G1 phase or S phase (time −3) and exposed to IR (4 Gy) 3 h after release (time 0). (*Right* panels) DNA repair was evaluated as in *A*. (*Left* panels) Cell cycle distributions are presented.

Given that levels of dNTP pools are higher during S phase than during G1 phase (Hakansson et al. 2006), recruitment of RNR at damage sites may function at a specific phase of the cell cycle where dNTP pools are low. To address this issue, we synchronized cells at S phase or G1 phase by arrest and release of thymidine or nocodazole, respectively. Recruitment of wild-type RRM1 at a DSB site was observed at both G1 and S phase (Supplemental Fig. S10). However, a comet assay revealed that A776CΔ781-C failed to rescue the impaired DNA repair in RRM1-depleted cells at G1 phase, but not at S phase (Fig. 4E). Consistently, RRM1 mutation of Tip60 binding slightly sensitizes cells to Zeocin (Supplemental Fig. S11A), which causes DNA strand breaks, but not to MMC (Supplemental Fig. S11B), which can cause interstrand cross-linking repaired mainly at S–G2 phase. Intriguingly, this G1-phase-specific impairment of DNA repair was restored when excess amounts of dADP, dGDP, dCDP, and dUMP (250 μM) were supplied in the culture medium (Supplemental Fig. S12). These results suggested that recruitment of RNR was required specifically for effective DNA repair in cells with low levels of dNTPs.

The present study suggests that the RNR recruitment to DSB sites likely provides mechanistic insights into the regulatory events that ensure a balanced supply of dNTPs during mammalian DNA repair. RNR appears to form a complex with Tip60 independently of DNA damage. Thus, it is possible that the RNR–Tip60 complex might have an alternative function, such as regulation of transcription. In response to DNA damage, regulation of the RNR subunit by Wtm1 and Dif1 in budding yeast is radically different in terms of cellular localization (Lee and Elledge 2006; Lee et al. 2008) from that observed in the present study; however, important changes in the subcellular localization of RNR might be conserved. Given that Tip60 is a key regulator of DNA damage responses, the concomitant recruitment of RNR at damage sites suggests the presence of a synthetic regulatory mechanism for DNA repair in mammals.

Materials and methods

Antibodies

Antibodies used were as follows: α-Rad51 (Ab-1, Oncogene Research Products), α-RRM1 (sc-11733 and sc-11731, Santa Cruz Biotechnologies), α-HA (11 666 606 001, Roche Applied Sciences; and PM002, MBL), α-Myc (sc-40 and sc-789, Santa Cruz Biotechnologies), α-RRM2(sc-10844, Santa Cruz Biotechnologies), α-GST (sc-459, Santa Cruz Biotechnologies), α-Chk1 (sc-8408, Santa Cruz Biotechnologies), α-IKKα (sc-7182, Santa Cruz Biotechnologies), α-Orc2 (sc-13238, Santa Cruz Biotechnologies), α-ATM (sc-23921, Santa Cruz Biotechnologies), α-ATMp1981 (no. 4526, Cell Signaling), α-acetylated histone H4 (no. 06-866, Upstate Biotechnologies), and α-phospho-histone H2AX (411-pc-020, TREVIGEN; and 05-636, Upstate Biotechnologies). Anti-Tip60 rabbit polyclonal antibodies were generated by immunization with recombinant GST-His-Tip60 produced in insect cells, and the serum obtained was affinity-purified using a GST-His-Tip60 column.

Two-hybrid interaction assays

The *pGBKT7-RRM1* plasmid was generated by insertion of the full-length human *RRM1*-encoding sequence. *pGBKT7-RRM1* was transformed into

the yeast strain AH101 and mated with yeast Y187 pretransformed with a HeLa cell cDNA library (BD Biosciences). The deletion mutants of RRM1 and Tip60 were amplified by PCR using specific sets of primers. Primer sequences are supplied in the Supplemental Material.

Affinity purification of Tip60 complex

Affinity purification of Tip60 complex was performed as described previously (Ikura et al. 2000, 2007). For the induction of DNA damage, cells were γ-irradiated (12 Gy) after centrifugation.

In situ detergent extraction and immunofluorescence analysis

Immunofluorescence on paraformaldehyde-fixed cells was performed according to a previous report (Green and Almouzni 2003), using the indicated antibodies.

Microirradiation

Microirradiation was performed as described previously (Ikura et al. 2007). In brief, GM02063 cells were maintained on the microscope stage in a Chamlide TC live-cell chamber system (Live Cell Instrument) at 37°C. Microirradiation was performed using an LSM510 confocal microscope (Carl Zeiss). Sensitization of cells was performed by incubating the cells for 20 h in medium containing 2.5 μM deoxyribosylthymine and 0.3 μM bromodeoxyuridine (Sigma), and then staining with 2 μg/mL Hoechst 33258 (Sigma) for 10 min before UVA microirradiation. The 364-nm line of the UVA laser was used for microirradiation (three pulses at 30 μW). Samples were examined with a Zeiss Axioplan 2 equipped with a charge-coupled device camera AxioCam MRm controlled by Axiovision software (Zeiss).

Knockdown experiments

HeLa cells or *STEFKu70*$^{-/-}$*phprt-DR-GFP* cells were transfected with either control siRNA (Silencer Negative Control #1, Ambion 4611), siRNAs for human Tip60 (sc-37966, Santa Cruz Biotechnologies), mouse Tip60-1 (sc-37967, Santa Cruz Biotechnologies), mouse Tip60-2 (D-057795-02-0010, Dharmacon), or RRM1 (GGAUCGCUGUCUCUAA CUUtt) using Lipofectamine 2000 reagent (Invitrogen).

Subcellular fractionation and Mnase treatment

Subcellular fractionation was performed according to a previous report (Mendez and Stillman 2000). The isolated chromatin fraction (1×10^6 cells) was treated with Mnase (15 U) for 30 min at 37°C.

Establishment of STEFKu70$^{-/-}$ cells containing a phprt-DR-GFP cassette

The *phprt-DR-GFP* vector (10 μg) was linearized with PvuI and transfected into *STEFKu70*$^{-/-}$ cells. Cells were selected with 1.25 μg/mL puromycin for 12 d, and single colonies were screened by Southern blotting using puromycin cDNA as a probe. Clones having only one copy of the *phprt-DR-GFP* cassette were used for experiments.

Establishment of Tet-on HeLa cells expressing NLS-RC1

pcDNA4/TO-NLS-RC1 (10 μg) was linearized with XhoI and transfected into HeLa T-Rex cells (Invitrogen). Positive clones were selected with Zeocin (250 μg/mL) and Blastcidin (5 μg/mL) for 12 d and screened by immunoblotting using anti-HA antibodies for the detection of NLS-RC1 induction in the presence of tetracycline (1 μg/mL).

Generation of adenoviruses expressing I-SceI endonuclease

The full-length *I-SceI* fragment harboring the *CAG* promoter and poly A signal was subcloned into *pAd/PL-DEST* (Invitrogen). Adenoviruses expressing I-SceI were generated according to the manufacturer's protocol (Invitrogen).

ChIP assay

A population of *STEFKu70*$^{-/-}$cells (1×10^7) containing *phprt-DR-GFP* cells infected with adenoviruses expressing I-SceI was cross-linked with 1% formaldehyde for 10 min at 37°C. ChIP assays were performed essentially as described (Shimada et al. 2008). Precipitated DNA was resuspended in 50 μL of water and analyzed by quantitative real-time PCR with the ABI PRISM7000 system using Power SYBR Green PCR Master Mix (Applied Biosystems) as described (Katsuno et al. 2009). Primers used for detection of the *I-SceI* break site were indicated in Figure 2A. As an internal control for normalization of the specific fragments amplified, mouse GAPDH locus was amplified using whole genomic DNAs with mGAPDH-F and mGAPDH-R. Primer sequences are supplied in the Supplemental Material.

Comet assay

Alkaline comet assays were performed using a Trevigen's Comet Assay kit (4250-050-k) according to the manufacturer's instructions. DNA was stained with SYBR Green, and slides were photographed digitally (Nikon Eclipse E800 lens and Fuji CCD camera). Tail moments were analyzed as reported previously (Park et al. 2006) using TriTek Comet Score Freeware.

Measurement of DNA damage sensitivity

Tet-on HeLa cells expressing NLS-RC1-HA or NLS-GFP-HA were irradiated with varying doses of IR in the presence or absence of doxycycline (1 μg/mL), and then washed with PBS. Eight days after an additional incubation, surviving colonies were counted, and their relative numbers were expressed as percentages of the untreated cells ($n = 3$).

RNR assay

Insect cells were coinfected with baculoviruses expressing wild-type RRM1 or its mutants, and with those expressing wild-type RRM2. RNR complexes were immunopurified, and their activities were determined according to a method reported previously (Fukushima et al. 2001). Amounts of wild-type RRM1 protein or its mutant proteins were determined by SDS-PAGE and used for calculating specific activities.

Cell cycle synchronization

For synchronization of cells at S phase, knockout–knock-in HeLa cells expressing wild-type or A776CΔ781-C RRM1-HA were first synchronized at the G1/S boundary by exposure to 2.5 mM thymidine for 16 h, and then released into S phase by wash-out of thymidine with PBS and the addition of 20% FBS containing DMEM. Cells were then exposed to IR 3 h after release. For synchronization of cells at G1 phase, knockout–knock-in HeLa cells were synchronized at M phase by exposure to 100 ng/mL nocodazole for 16 h and released into G1 phase by wash-out of nocodazole with PBS and addition of 20% FBS containing DMEM. Cells were then exposed to IR 3 h after release.

Acknowledgments

We thank M. Delhase for critical reading of the manuscript; M. Jasin for hprt-DR-GFP and pCBASce vectors; M. Fukushima for critical advice on the RNR assay; A. Kurimasa for *STEFKu70*$^{-/-}$ MEFs; K. Murata, C. Namikawa-Yamada, and H. Kojima for technical assistance; and M. Inagaki and H. Goto for fluorescence microscopy. This work was supported in part by the Ministry of Education, Science, Sports, and Culture of Japan through Grants-in-Aid for Scientific Research (B) (to M.N.) and (C) (to H.N.), the YASUDA Medical Foundation (to M.N.), and the Sagawa Cancer Foundation (to M.N.).

References

Dong Q, Wang TS. 1995. Mutational studies of human DNA polymerase α. Lysine 950 in the third most conserved region of α-like DNA polymerases is involved in binding the deoxynucleoside triphosphate. *J Biol Chem* **270:** 21563–21570.

Fukushima M, Fujioka A, Uchida J, Nakagawa F, Takechi T. 2001. Thymidylate synthase (TS) and ribonucleotide reductase (RNR) may be involved in acquired resistance to 5-fluorouracil (5-FU) in human cancer xenografts in vivo. *Eur J Cancer* **37:** 1681–1687.

Green CM, Almouzni G. 2003. Local action of the chromatin assembly factor CAF-1 at sites of nucleotide excision repair in vivo. *EMBO J* **22:** 5163–5174.

Guittet O, Hakansson P, Voevodskaya N, Fridd S, Graslund A, Arakawa H, Nakamura Y, Thelander L. 2001. Mammalian p53R2 protein forms an active ribonucleotide reductase in vitro with the R1 protein, which is expressed both in resting cells in response to DNA damage and in proliferating cells. *J Biol Chem* **276:** 40647–40651.

Hakansson P, Hofer A, Thelander L. 2006. Regulation of mammalian ribonucleotide reduction and dNTP pools after DNA damage and in resting cells. *J Biol Chem* **281:** 7834–7841.

Ikura T, Ogryzko VV, Grigoriev M, Groisman R, Wang J, Horikoshi M, Scully R, Qin J, Nakatani Y. 2000. Involvement of the TIP60 histone acetylase complex in DNA repair and apoptosis. *Cell* **102:** 463–473.

Ikura T, Tashiro S, Kakino A, Shima H, Jacob N, Amunugama R, Yoder K, Izumi S, Kuraoka I, Tanaka K, et al. 2007. DNA damage-dependent acetylation and ubiquitination of H2AX enhances chromatin dynamics. *Mol Cell Biol* **27:** 7028–7040.

Imaizumi T, Jean-Louis F, Dubertret ML, Bailly C, Cicurel L, Petchot-Bacque JP, Dubertret L. 1996. Effect of human basic fibroblast growth factor on fibroblast proliferation, cell volume, collagen lattice contraction: In comparison with acidic type. *J Dermatol Sci* **11:** 134–141.

Johnson RE, Trincao J, Aggarwal AK, Prakash S, Prakash L. 2003. Deoxynucleotide triphosphate binding mode conserved in Y family DNA polymerases. *Mol Cell Biol* **23:** 3008–3012.

Katsuno Y, Suzuki A, Sugimura K, Okumura K, Zineldeen DH, Shimada M, Niida H, Mizuno T, Hanaoka F, Nakanishi M. 2009. Cyclin A–Cdk1 regulates the origin firing program in mammalian cells. *Proc Natl Acad Sci* **106:** 3184–3189.

Kraynov VS, Showalter AK, Liu J, Zhong X, Tsai MD. 2000. DNA polymerase β: Contributions of template-positioning and dNTP triphosphate-binding residues to catalysis and fidelity. *Biochemistry* **39:** 16008–16015.

Lee YD, Elledge SJ. 2006. Control of ribonucleotide reductase localization through an anchoring mechanism involving Wtm1. *Genes & Dev* **20:** 334–344.

Lee YD, Wang J, Stubbe J, Elledge SJ. 2008. Dif1 is a DNA-damage-regulated facilitator of nuclear import for ribonucleotide reductase. *Mol Cell* **32:** 70–80.

Mendez J, Stillman B. 2000. Chromatin association of human origin recognition complex, cdc6, and minichromosome maintenance proteins during the cell cycle: Assembly of prereplication complexes in late mitosis. *Mol Cell Biol* **20:** 8602–8612.

Murr R, Loizou JI, Yang YG, Cuenin C, Li H, Wang ZQ, Herceg Z. 2006. Histone acetylation by Trrap–Tip60 modulates loading of repair proteins and repair of DNA double-strand breaks. *Nat Cell Biol* **8:** 91–99.

Niida H, Katsuno Y, Banerjee B, Hande MP, Nakanishi M. 2007. Specific role of Chk1 phosphorylations in cell survival and checkpoint activation. *Mol Cell Biol* **27:** 2572–2581.

Nordlund P, Reichard P. 2006. Ribonucleotide reductases. *Annu Rev Biochem* **75:** 681–706.

Park JH, Park EJ, Lee HS, Kim SJ, Hur SK, Imbalzano AN, Kwon J. 2006. Mammalian SWI/SNF complexes facilitate DNA double-strand break repair by promoting γ-H2AX induction. *EMBO J* **25:** 3986–3997.

Pierce AJ, Hu P, Han M, Ellis N, Jasin M. 2001. Ku DNA end-binding protein modulates homologous repair of double-strand breaks in mammalian cells. *Genes & Dev* **15:** 3237–3242.

Pontarin G, Fijolek A, Pizzo P, Ferraro P, Rampazzo C, Pozzan T, Thelander L, Reichard PA, Bianchi V. 2008. Ribonucleotide reduction is a cytosolic process in mammalian cells independently of DNA damage. *Proc Natl Acad Sci* **105:** 17801–17806.

Reichard P. 1993. From RNA to DNA, why so many ribonucleotide reductases? *Science* **260:** 1773–1777.

Shimada M, Niida H, Zineldeen DH, Tagami H, Tanaka M, Saito H, Nakanishi M. 2008. Chk1 is a histone H3 threonine 11 kinase that regulates DNA damage-induced transcriptional repression. *Cell* **132:** 221–232.

Zhang Z, Yang K, Chen CC, Feser J, Huang M. 2007. Role of the C terminus of the ribonucleotide reductase large subunit in enzyme regeneration and its inhibition by Sml1. *Proc Natl Acad Sci* **104:** 2217–2222.

—Review—

iPS細胞への遺伝子導入を用いた分化誘導の最適化

川端健二,*,[a,b] 田代克久,[a] 水口裕之[a,c]

Differentiation of Functional Cells from iPS Cells by Efficient Gene Transfer

Kenji KAWABATA,*,[a,b] Katsuhisa TASHIRO,[a] and Hiroyuki MIZUGUCHI[a,c]

[a]*Laboratory of Stem Cell Regulation, National Institute of Biomedical Innovation, 7–6–8 Saito-Asagi, Ibaraki, Osaka 567–0085, Japan,* [b]*Department of Biomedical Innovation and* [c]*Department of Biochemistry and Molecular Biology, Graduate School of Pharmaceutical Sciences, Osaka University, 1–6 Yamadaoka, Suita, Osaka 565–0871, Japan*

(Received July 20, 2010)

Induced pluripotent stem (iPS) cells, which are generated from somatic cells by transducing four genes, are expected to have broad application to regenerative medicine. Although establishment of an efficient gene transfer system for iPS cells is considered to be essential for differentiating them into functional cells, the detailed transduction characteristics of iPS cells have not been examined. By using an adenovirus (Ad) vector containing the cytomegalovirus enhancer/beta-actin (CA) promoters, we have developed an efficient transduction system for mouse mesenchymal stem cells and embryonic stem (ES) cells. Also, we applied our transduction system to mouse iPS cells and investigated whether efficient differentiation could be achieved by Ad vector-mediated transduction of a functional gene. As in the case of ES cells, the Ad vector could efficiently transduce transgenes into mouse iPS cells. We found that the CA promoter had potent transduction ability in iPS cells. Moreover, exogenous expression of a PPARγ gene or a Runx2 gene into mouse iPS cells by an optimized Ad vector enhanced adipocyte or osteoblast differentiation, respectively. These results suggest that Ad vector-mediated transient transduction is sufficient to promote cellular differentiation and that our transduction methods would be useful for therapeutic applications based on iPS cells.

Key words——regenerative medicine; induced pluripotent stem (iPS) cell; adenovirus vector; mesenchymal stem cell; embryonic stem (ES) cell

1. はじめに

幹細胞（stem cells）は自己複製能と分化多能性という大きく2つの特徴を有する細胞であり，目的の細胞へ分化させることにより創薬や再生医療への応用が期待されている．再生医療への応用が期待されている幹細胞には，造血幹細胞，神経幹細胞，間葉系幹細胞，ES（embryonic stem）細胞，iPS（induced pluripotent stem）細胞などがある．このうち，ES細胞は受精卵（胚）から樹立され，iPS細胞は体細胞に4種の遺伝子（Oct-3/4m Sox2, Klf4, c-Myc）を導入することにより作製される．しかしながら，ES細胞やiPS細胞を直接生体に移植するには困難な場合も多く，マウス生体に投与するとランダムに分化しテラトーマ（奇形腫）を形成する．したがって，治療目的には幹細胞を *in vitro* で目的の細胞に分化させた後生体に移植することが望ましいと考えられる．幹細胞を骨，心筋，脂肪，血液などの目的の細胞に分化させるには，培養液に特定のサイトカインや増殖因子等の液性因子を加える方法がとられているが分化効率は十分ではない．そこで，われわれは各種幹細胞に機能遺伝子を導入することにより効率よく分化させることができないかと考え研究を進めている．一般に，幹細胞は遺伝子導入が困難であり，リポフェクション法やレトロウイルスベクター系など通常用いられる方法では十分な導入効率が得られない．われわれは高効率かつ一過性に目的遺伝子を発現させることができるアデノウイルス（Ad）ベクターを用いて機能遺伝子を導入

[a]独立行政法人医薬基盤研究所幹細胞制御プロジェクト（〒567–0085 大阪府茨木市彩都あさぎ7–6–8），[b]大阪大学大学院薬学研究科医薬基盤科学分野，[c]同分子生物学分野（〒565–0871 大阪府吹田市山田丘1–6）
*e-mail: kawabata@nibio.go.jp

本総説は，日本薬学会第130年会シンポジウムS19で発表したものを中心に記述したものである．

することにより，幹細胞の分化誘導効率を向上させることを目指した．

2. 間葉系幹細胞への遺伝子導入

間葉系幹細胞は骨髄由来のストローマ細胞であり，骨，軟骨，脂肪，心筋系列などの中胚葉系細胞に分化することができ，未分化状態で細胞を容易に増殖させることができる．[1] また，最近では，間葉系幹細胞は神経細胞，肝細胞，インスリン産生細胞などの外胚葉や内胚葉系の細胞へも分化するという報告もあり，再生医療や組織工学への応用が強く期待されている．間葉系幹細胞の分化を制御する手段の1つとして，細胞分化に関与する遺伝子を導入することが挙げられる．Ad ベクターを用いた間葉系幹細胞への遺伝子導入も試みられてきたが，間葉系幹細胞は Ad 受容体 CAR (coxsackievirus and adenovirus receptor) を発現していないためにその導入効率は極めて低く，遺伝子導入には高タイターのベクターを必要としていた．[2,3] われわれは，独自に開発した種々のファイバー改変型 Ad ベクターを用いて間葉系幹細胞にレポーター遺伝子を導入し，その発現効率を比較検討した．[4,5] 間葉系幹細胞を多く含有する画分であるマウス骨髄ストローマ細胞を用いて遺伝子導入効率を測定した結果，間葉系幹細胞にはファイバーにポリリジン残基を挿入した K7 型ベクターが最も適しており，従来型ベクターの 100 倍以上の遺伝子導入効率を示すことが明らかとなった [Figs. 1(A) and (B)]．RGD 型ベクターは従来型ベクターに比較し 10 倍程度の導入効率を示した．また，種々のプロモーターを用いて比較検討したところ，CA プロモーターが最適であった [Fig. 1 (C)]．したがって，間葉系幹細胞には CA プロモーターを有する K7 型 Ad ベクターを用いることにより最も高効率に遺伝子導入できることが明らかとなった．間葉系幹細胞は様々な系列の細胞に分化するというだけではなく，担がんマウスに投与された場合には腫瘍に集積する性質を有している．[6] し

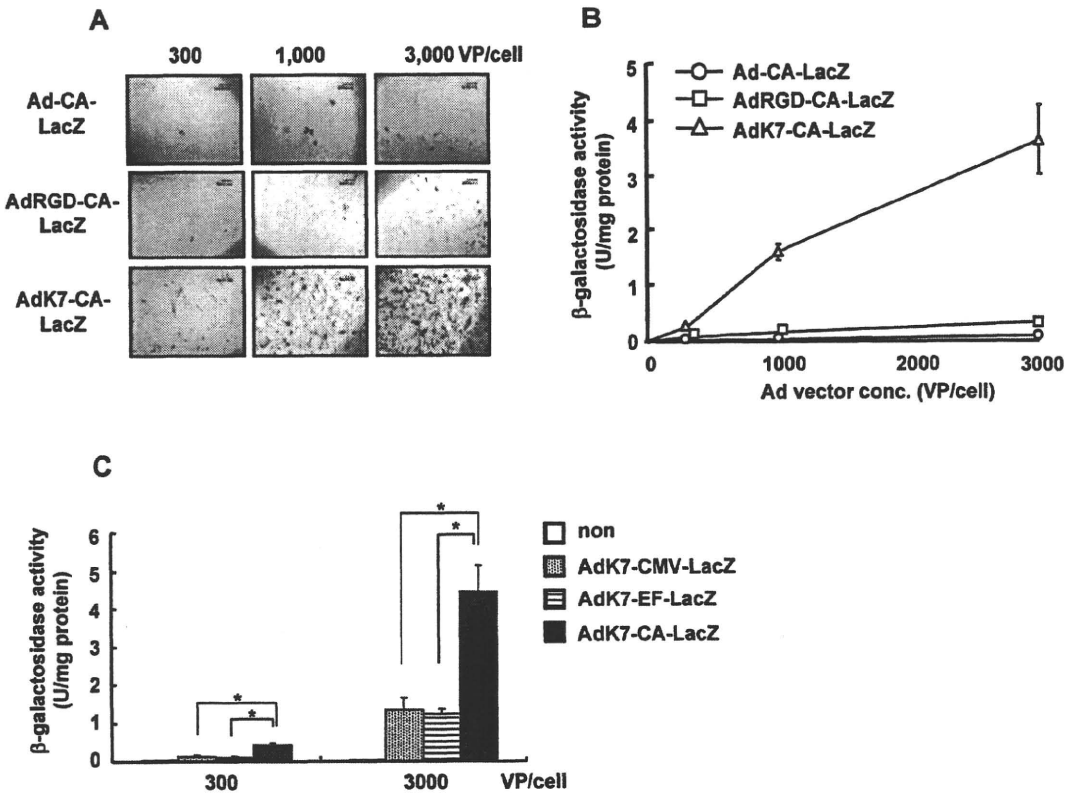

Fig. 1. Gene Transduction Efficiency in Mouse Primary BMSCs by Various Types of Ad Vectors

Mouse primary BMSCs were transduced with the indicated doses of LacZ-expressing Ad vectors for 1.5 h. Two days later, (A) X-gal staining and (B) luminescence assay were carried out. Similar results of X-gal staining were obtained in three independent experiments. Scale bar indicates 200 μm. (C) Optimization of promoter activity in BMSCs using LacZ-expressing AdK7. BMSCs were transduced with each Ad vector at 300 or 3000 VP/cell, and LacZ expression in the cells was measured. The data (B and C) are expressed as mean±S.D. (n=3). *p<0.01.

たがって，間葉系幹細胞は分化させた細胞自身を治療に利用するだけでなく，抗腫瘍性サイトカイン等を発現する間葉系幹細胞をがんに対する細胞治療薬として利用できる可能性があり，現在検討している．

3. 間葉系幹細胞の分化誘導

間葉系幹細胞への遺伝子導入にはCAプロモーターを有したK7型Adベクターが最適であることが明らかとなったので，次に本ベクターを用いて機能遺伝子を導入し分化誘導効率を向上させることを試みた．Runx2はRuntファミリーに属する転写因子であり，Runx2遺伝子欠損マウスは骨芽細胞分化が初期で停止し骨形成が欠損することが知られている．[7] そこで，Runx2遺伝子をマウス骨髄ストローマ細胞に導入した結果，従来の分化誘導法と比較しアルカリホスファターゼ活性の上昇及びカルシウムの沈着がみとめられ，著明に骨芽細胞への分化誘導効率が促進されることが明らかとなった［Figs. 2(A) and (B)］．また，それに伴い，タイプIコラーゲン，オステリクス，オステオカルシン等の骨芽細胞マーカー遺伝子の発現も上昇した［Fig. 2(C)］．さらに，このようにして分化誘導した骨芽細胞をマウスに移植したところ，Fig. 3に示すように異所性の骨形成がみとめられ，*in vivo*においても機能を有していることが示された．以上より，本ベクターは*in vitro*及び*in vivo*において間葉系細胞を効率よく骨芽細胞へ分化誘導するのに適したベクターであることが示された．

4. マウスES細胞及びマウスiPS細胞への遺伝子導入

ES細胞は胚盤胞内部細胞塊由来の細胞であり，無限に増殖するとともにすべての機能細胞に分化する性質を有する．一方，iPS細胞は体細胞に4種の遺伝子（Oct-3/4, c-myc, Sox2, Klf4）を同時に導入することにより得られる人工多能性幹細胞であり，倫理的な問題を回避できることから再生医療への応用が大きく期待されている．[8] しかしながら，これら幹細胞の分化を自由に制御する技術はいまだ確立されておらず，その原因の1つとして効率よい遺伝子導入法が確立されていないことが挙げられる．これまで，ES細胞に対しては，プラスミドDNAを用いたエレクトポレーション法（プラスミドDNAを電気的刺激により細胞内に導入し，染色体にわずかに目的遺伝子と薬剤耐性遺伝子が組み込まれた細胞を薬剤で選択する方法），[9] レトロウイルスベクター，[10] レンチウイルスベクター，[11] ポリオーマウイルスの複製機構を利用したスーパートランスフェクション法（ポリオーマウイルスの複製起点を含んだプラスミドDNAがマウスES細胞ではエピゾーマルに増幅できる性質を利用した方法）[12] などが外来遺伝子導入法として用いられてきた．しかしながら，これらは半永久的に導入遺伝子を発現し続ける方法であり，ES細胞やiPS細胞の分化制御，特に医療目的などの細胞分化後には発現を停止させたい場合には好ましくない．Adベクターは導入遺伝子が宿主染色体へ組込まれることなく，染色体外にエピゾームとして存在することから（増幅しない），遺伝子発現が一過性であり，ES細胞やiPS細胞を目的の機能細胞に分化させた後は導入遺伝子の発現が消失するものと期待される．そこで，筆者らは，マウスES細胞及びiPS細胞に最も適したAdベクターによる遺伝子導入法の確立を試みた．その結果，マウスES細胞やiPS細胞はAd受容体CARを高発現しており，従来型アデノウイルスベクターが最適であることが明らかとなった．[13,14] また，RSV, CMV, CA（β-actin promoter/CMV enhancer），EF-1αの4種のプロモーターを用いて検討した結果，ES細胞及びiPS細胞ではCA及びEF-1αプロモーターを用いた場合にのみ遺伝子発現がみられ，RSVやCMVプロモーターはほとんど機能しなかった［Fig. 4(A)］．これまでAdベクターはES細胞への遺伝子導入には不適と考えられてきたが，これは多くの場合，最も一般的に用いられているCMVプロモーターを用いて検討されてきたためであり，ウイルスの細胞へのエントリー自体には問題がないことが示された．ただし，CAプロモーターを用いた場合にはES細胞のみならずその支持細胞（フィーダー細胞）である胚繊維芽細胞にも遺伝子発現がみられたのに対し，EF-1αプロモーターを用いた場合にはほぼES細胞特異的に遺伝子発現可能であった．これは，EF-1αプロモーターの活性が胚繊維芽細胞に比べES細胞において相対的に高いことが原因と考えられる．したがって，目的により両プロモーターを使い分けることによって，再生医療への幅広い応用が期待できる．

Adベクターを導入することによりES細胞やiPS細胞が有する本来の性質が失われると再生医療

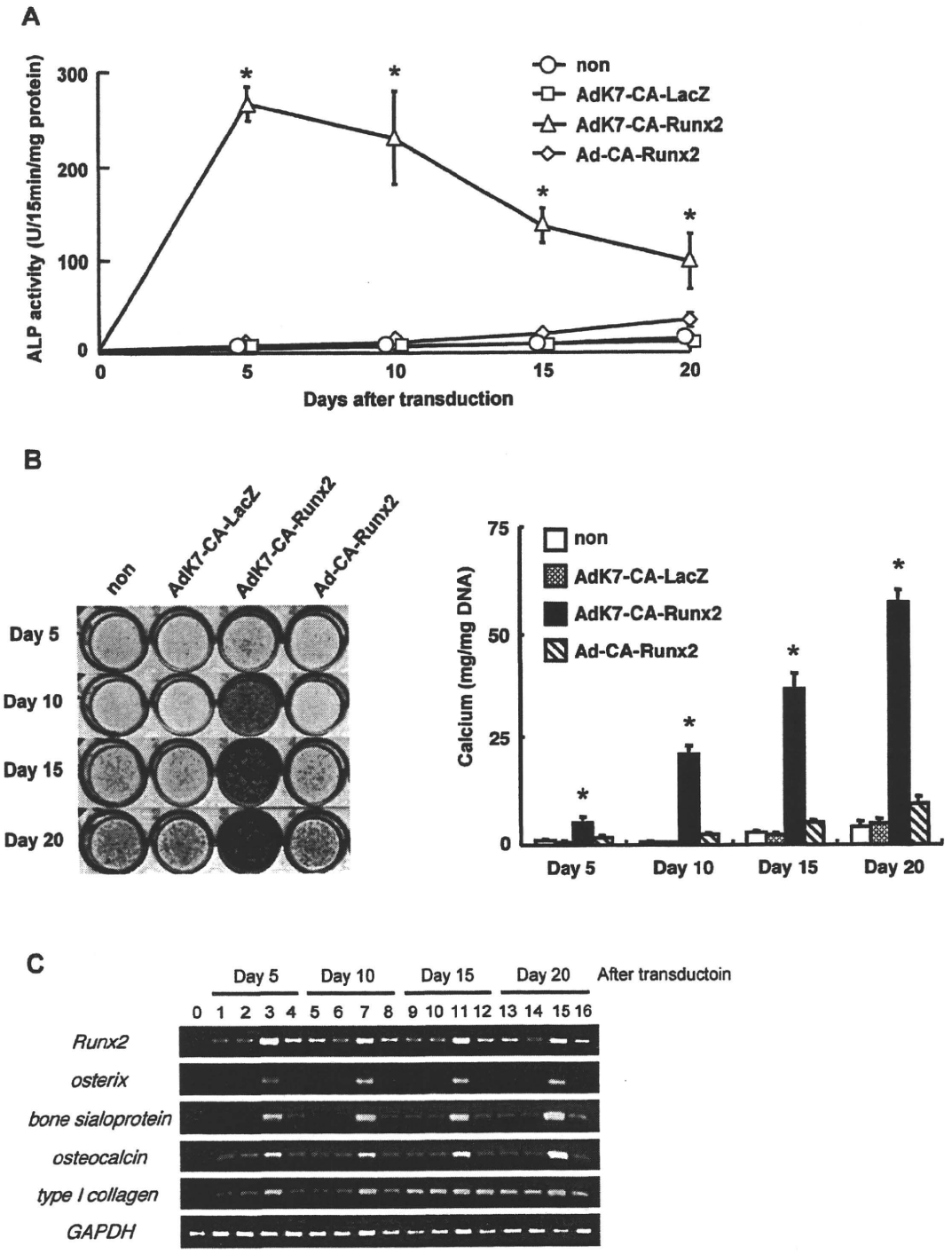

Fig. 2. Promotion of *in Vitro* Osteoblastic Differentiation in BMSC Transduced with AdK7-CA-Runx2

BMSCs were transduced with each Ad vector at 3000 VP/cell for 1.5 h, and were cultured for the indicated number of days. (A) Alkaline phosphatase activity, (B, left) matrix minerarization, and (B, right) calcium deposition in the cells was determined as described in Materials and Methods. The data are expressed as mean±S.D. (n=3). *p<0.01 as compared with non-, AdK7-CA-LacZ-, or Ad-CA-Runx2-transduced cells. (C) RT-PCR was carried out using primers for Runx2, osterix, bone sialoprotein, osteocalcin, collagen type I, and GAPDH. Lane 0: non-treated BMSCs; lanes 1, 5, 9, and 13: BMSCs with osteogenic supplements (OS); lanes 2, 6, 10, and 14: BMSCs with OS plus AdK7-CA-LacZ; lanes 3, 7, 11, and 15: BMSCs with OS plus AdK7-CA-Runx2; lanes 4, 8, 12, and 16: BMSCs with OS plus Ad-CA-Runx2.

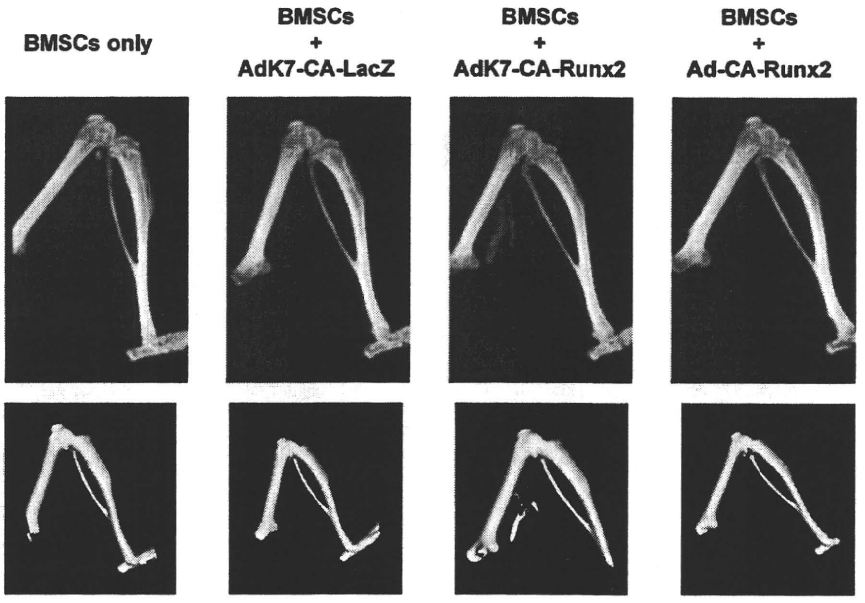

Fig. 3. *In vivo* Ectopic Bone Formation of Mouse BMSCs by AdK7-mediated Runx2 Gene Transduction

BMSCs were transduced with indicated Ad vectors at 3000 VP/cell for 1.5 h. On the following day, cells (2×10^6 cells) were suspended in PBS and injected into the hind limb biceps muscle of nude mice. Four weeks later, bone formation was analyzed by the microCT system. Similar results were obtained in two independent experiments. Upper, X-ray images; lower, 3D reconstitution images.

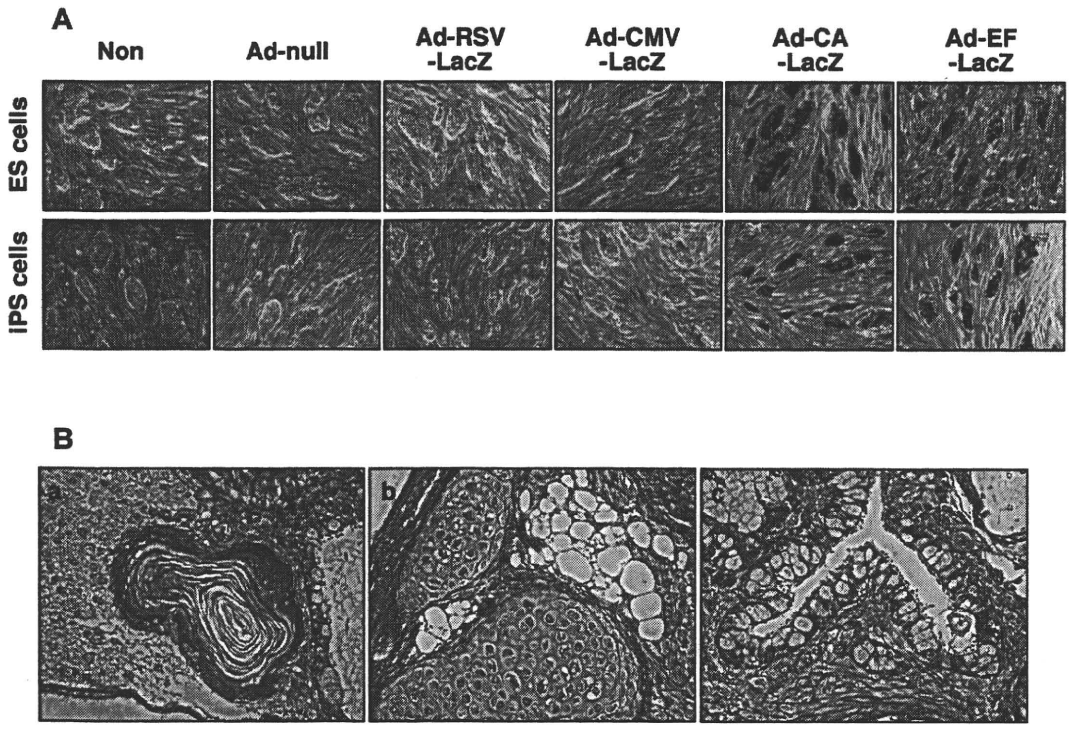

Fig. 4. Efficient Transgene Expression in Mouse iPS Cells by Using an Ad Vector Containing the CA and the EF-1α Promoter

(A) Mouse ES cells or iPS cells were transduced with LacZ-expressing Ad vector at 3000 VP/cell. On the following day, X-gal staining was carried out. Similar results of X-gal staining were obtained in three independent experiments. (B) Paraffin sections of the teratomas derived from Ad-CA-mCherry-transduced iPS cells were prepared, and sections were stained with hematoxylin and eosin. a, ectoderm (epidermis); b, mesoderm (cartilage and adipocyte); c, endoderm (gut epithelium).

への応用は困難となる．そこで，三胚葉への分化能が保持されているかどうかを検討するために，Adベクター導入後のiPS細胞を用いてテラトーマ形成実験を行った［Fig. 4(B)］．その結果，遺伝子導入されたiPS細胞はもとのiPS細胞と同様に外胚葉・中胚葉・内胚葉いずれにも分化可能であることが明らかとなり，Adベクターは ES細胞やiPS細胞の分化能を妨げることなく，効率よく遺伝子導入ができるベクターであることが明らかとなった．

5. 遺伝子導入によるES細胞の分化制御

最適化されたAdベクターを用いてES細胞に機能遺伝子を導入し，実際にES細胞の分化を制御できるかどうかについて検討した．マウスES細胞はフィーダー細胞由来のサイトカインLIF（leukemia inhibitory factor）がその未分化維持に必須であることが知られている．LIFは受容体に結合後，下流のSTAT3（signal transducer and activator of transcription 3）を介してシグナルを伝達する．そこで，EF-1αプロモーターを有した従来型Adベクターを用いてSTAT3のdominant-negative変異体(STAT3F)のcDNAをマウスES細胞に導入することにより，LIFの下流シグナルを阻害させたところ，LIF存在下でもES細胞は三胚葉すべての細胞に分化することが明らかとなった［Fig. 5(A)］．ES細胞の未分化維持にはLIF以外にもNanogなどの転写因子が必須であることが明らかとなっている．そこで，先述のベクターを用いてSTAT3FとNanogを同時に発現させたところ，STAT3Fによる細胞分化シグナルがNanog発現により阻害され，ES細胞は未分化状態を維持し続けた［Fig. 5(B)］．したがって，Adベクターを用いることでES細胞の分化を自由に制御できる可能性が示された．

6. ES細胞及びiPS細胞の高効率分化誘導

Adベクターを用いた遺伝子導入技術が分化誘導系に応用できるかどうかを検討するために，マウスES細胞及びiPS細胞へ機能遺伝子を導入することを試みた．ES細胞及びiPS細胞からの分化モデルとして脂肪細胞への分化誘導を行うとともに，脂肪細胞分化に必須の遺伝子であるPPARγ（peroxisome proliferator-activated receptor gamma）遺伝子[15]をES細胞及びiPS細胞へ導入することにより，脂肪細胞への分化効率が上昇するかどうかを検討した．両細胞へLacZ遺伝子（コントロール）又

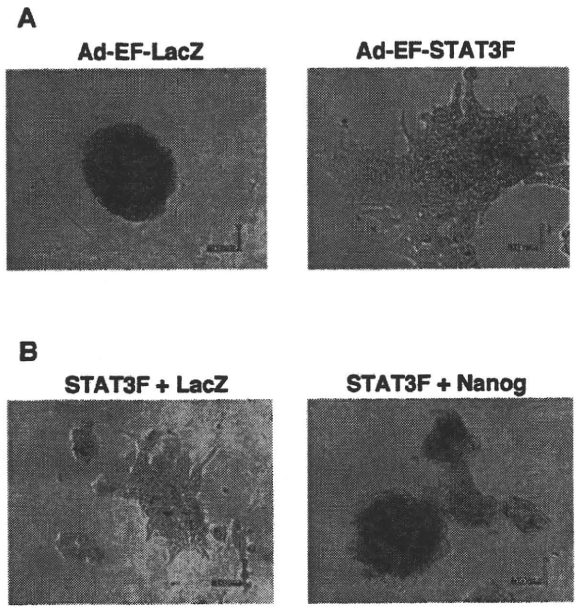

Fig. 5. Introduction of Functional Genes into Mouse ES Cells by Ad Vectors Containing EF-1α Promoter

Mouse ES cells (1×10^4 cells) were seeded, and on the following day, the cells were transduced with 3000 VP/cell of Ad-EF-LacZ or Ad-EF-STAT3F for 1.5 h (A). Mouse ES cells were also co-infected with 3000 VP/cell of Ad-EF-STAT3F and 3000 VP/cell of Ad-EF-lacZ or Ad-EF-Nanog for 1.5 h (B). On day 3, each cell was infected again by the same vectors. On day 5, alkaline phosphatase staining was performed. Alkaline phosphatase-positive cells indicate undifferentiated ES cells. Similar results were obtained in three independent experiments.

はPPARγ遺伝子を導入し，脂肪細胞分化用の液性因子（インスリン，デキサメタゾンなど）を含む培地中で15日間接着培養した．オイルレッドO染色により脂肪細胞への分化効率を評価した結果，iPS細胞の脂肪細胞への分化効率はES細胞の分化効率よりも低いものの，液性因子を作用させて培養することにより両細胞とも脂肪滴が観察された［Fig. 6(A)］．さらに，液性因子のみを用いた分化誘導法と比較し，液性因子を加えさらにAdベクターによるPPARγ遺伝子を導入したES細胞及びiPS細胞は，極めて効率よく脂肪細胞へ分化していることも示された．すなわち，従来の方法ではES細胞において約50%の細胞が，iPS細胞において20–30%の細胞がそれぞれオイルレッドOで染色されたのに対し，PPARγ遺伝子を導入したES細胞及びiPS細胞においては80–90%の細胞がオイルレッドOに染色された．また，Adベクターを用いたPPARγ遺伝子導入による脂肪細胞への分化効率の上昇は，脂肪細胞特異的なマーカー遺伝子の発現上昇によっても確認された．なお，LacZ遺伝子を導

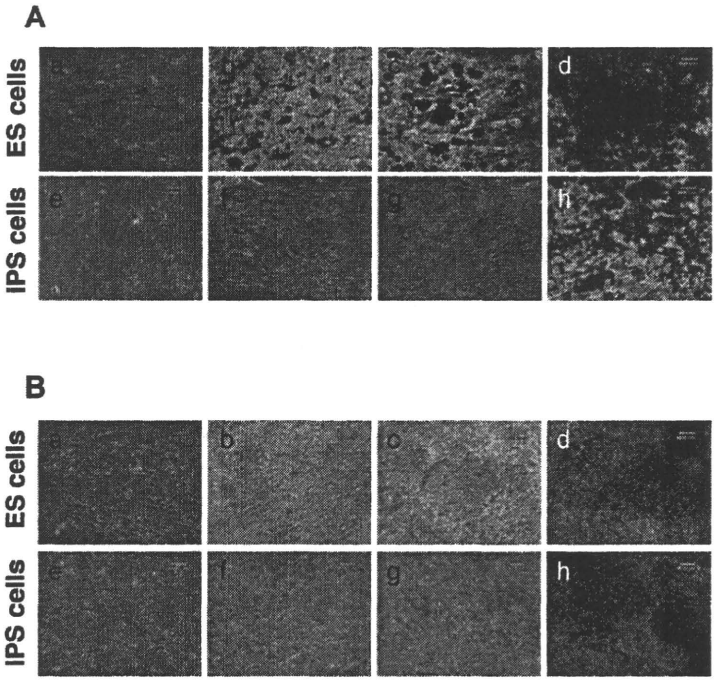

Fig. 6. Efficient Adipocytic or Osteoblastic Differentiation from Mouse ES Cells and iPS Cells by the Transduction of the PPARγ or Runx2 Gene

(A) ES-EBs or iPS-EBs were transduced in triplicate with 10000 VP/cell of Ad-CA-LacZ or Ad-CA-PPARγ. After plating onto a gelatin-coated dish on day 7, ES-EBs and iPS-EBs were cultured for 15 days in the presence or absence of adipogenic supplements (AS). After cultivation, lipid accumulation was detected by oil red O staining. a, non-treated ES-EBs; b, ES-EBs with AS; c, ES-EBs with AS plus Ad-CA-LacZ; d, ES-EBs with AS plus Ad-CA-PPARγ; e, non-treated iPS-EBs; f, iPS-EBs with AS; g, iPS-EBs with AS plus Ad-CA-LacZ; h, iPS-EBs with AS plus Ad-CA-PPARγ. The scale bar indicates 60 μm. (B) ES-EBs or iPS-EBs were transduced in triplicate with 10000 VP/cell of Ad-CA-LacZ or Ad-CA-Runx2. After culturing for 15 days with or without osteogenic supplements (OS), matrix mineralization in the cells was detected by von Kossa staining. a, non-treated ES-EBs; b, ES-EBs with OS; c, ES-EBs with OS plus Ad-CA-LacZ; d, ES-EBs with OS plus Ad-CA-Runx2; e, non-treated iPS-EBs; f, iPS-EBs with OS; g, iPS-EBs with OS plus Ad-CA-LacZ; h, iPS-EBs with OS plus Ad-CA-Runx2. The scale bar indicates 60 μm.

入した細胞ではこのような分化効率の上昇はみとめられなかった．これらの結果から，マウスES細胞及びiPS細胞の脂肪細胞への分化効率はAdベクターを用いたPPARγ遺伝子の導入により改善できることが示された．

次に，Adベクターによる遺伝子導入がその他の細胞種への分化誘導系にも有用であるかどうかを検討するため，マウスES細胞及びiPS細胞から骨芽細胞への分化誘導を試みた．今回の分化誘導系においては前述したRunx2遺伝子をAdベクターにより発現させた．Ad-CA-Runx2をEB（embryoid body）へ3回作用させ，骨芽細胞分化用の液性因子（βグリセロリン酸，アスコルビン酸など）中で接着培養し，マウスES細胞及びiPS細胞由来の細胞が石灰化を生ずる骨芽細胞へ分化しているかどうかをvon Kossa染色により解析した．その結果，液性因子を作用させることにより石灰化が検出されたものの，その分化効率は低く，20%以下の細胞しか石灰化を起こしていなかった[Fig. 6(B)]．一方，Runx2遺伝子を導入したES細胞及びiPS細胞は，液性因子のみで培養した細胞及びLacZ遺伝子を導入した細胞と比較し，石灰化した細胞が著明に増加していること明らかとなった[Fig. 6(B)]．また，沈着した石灰化を定量化したところ，LacZ遺伝子導入群においては液性因子のみの誘導法と著差はみとめられなかったものの，Runx2遺伝子導入細胞においては約8倍，石灰化が上昇していた．これらの結果から，AdベクターによるRunx2遺伝子の導入によりマウスES細胞及びiPS細胞から骨芽細胞へ効率よく分化誘導可能であることが示された．このように最適化したAdベクターを用いたマウスES細胞及びiPS細胞への分化関連遺伝子の導入により，脂肪細胞及び骨芽細胞への分化効率を飛躍的に改善できることが示され，本遺伝子導入技術はマウスES細胞及びiPS細胞を用いた細胞分化研究に有用であると考えられた．

7. おわりに

これまでにもレトロウイルスベクターなどの恒常的遺伝子発現系を用いてES細胞から標的の細胞への分化誘導は行われてきた．しかしながら，これらの手法では機能遺伝子が染色体に挿入されるため治療用に適しておらず，一過性の遺伝子導入系の分化誘導が望まれていた．今回，われわれはAdベクターを用いたマウスES細胞及びiPS細胞への高効率遺伝子導入法を確立し，さらにその遺伝子導入技術を利用して分化関連遺伝子をマウスES細胞及びiPS細胞へ導入することにより特定の細胞へ効率よく分化誘導することに成功した．なお，異なるiPS細胞株についても今回と同様の結果が得られており，[14] 幅広いES細胞及びiPS細胞株に適用可能であることが示唆されている．また，今回は示していないが，分化が完了した細胞ではAdベクター由来の遺伝子発現はほとんどみとめられないことも確認している．[16] したがって，Adベクターは幹細胞を用いた分化誘導研究において，効率面だけでなく安全面においても非常に有用であると考えられる．現在，筆者らのグループではAdベクターを用いた遺伝子導入技術がその他の細胞種への分化誘導系へ応用可能かどうかに関して，マウス及びヒトのES細胞及びiPS細胞を用いて検討中である．一過性発現を示すAdベクターを用いた遺伝子導入技術は，幹細胞研究・再生医療研究において重要なツールになるものと考えられ，今後のますますの応用が期待される．

REFERENCES

1) Pittenger M. F., Mackay A. M., Beck S. C., Jaiswal R. K., Douglas R., Mosca J. D., Moorman M. A., Simonetti D. W., Craig S., Marshak D. R., *Science*, **284**, 143–147 (1999).
2) Conget P. A., Minguell J. J., *Exp. Hematol.*, **28**, 382–390 (2000).
3) Hung S. C., Lu C. Y., Shyue S. K., Liu H. C., Ho L. L., *Stem Cells*, **22**, 1321–1329 (2004).
4) Mizuguchi H., Sasaki T., Kawabata K., Sakurai F., Hayakawa T., *Biochem. Biophys. Res. Commun.*, **332**, 1101–1106 (2005).
5) Tashiro K., Kondo A., Kawabata K., Sakurai H., Sakurai F., Yamanishi K., Hayakawa T., Mizuguchi H., *Biochem. Biophys. Res. Commun.*, **30**, 127–132 (2009).
6) Studeny M., Marini F. C., Dembinski J. L., Zompetta C., Cabreira-Hansen M., Bekele B. N., Champlin R. E., Andreeff M., *J. Natl. Cancer Inst.*, **96**, 1593–1603 (2004).
7) Komori T., *J. Cell. Biochem.*, **95**, 445–453 (2005).
8) Takahashi K., Yamanaka S., *Cell*, **126**, 663–676 (2006).
9) Tompers D. M., Labosky P. A., *Stem Cells*, **22**, 243–249 (2004).
10) Cherry S. R., Biniszkiewicz D., van Parijs L., Baltimore D., Jaenisch R., *Mol. Cell. Biol.*, **20**, 7419–7426 (2000).
11) Gropp M., Itsykson P., Singer O., Ben-Hur T., Reinhartz E., Galun E., Reubinoff B. E., *Mol. Ther.*, **7**, 281–287 (2003).
12) Niwa H., Masui S., Chambers I., Smith A. G., Miyazaki J., *Mol. Cell. Biol.*, **22**, 1526–1536 (2002).
13) Kawabata K., Sakurai F., Yamaguchi T., Hayakawa T., Mizuguchi H., *Mol. Ther.*, **12**, 547–554 (2005).
14) Tashiro K., Inamura M., Kawabata K., Sakurai F., Yamanishi K., Hayakawa T., Mizuguchi H., *Stem Cells*, **27**, 1802–1811 (2009).
15) Tontonoz P., Hu E., Spiegelman B. M., *Cell*, **79**, 1147–1156 (1994).
16) Tashiro K., Kawabata K., Sakurai H., Kurachi S., Sakurai F., Yamanishi K., Mizuguchi H., *J. Gene Med.*, **10**, 498–507 (2008).

MT Open

Efficient Generation of Hepatoblasts From Human ES Cells and iPS Cells by Transient Overexpression of Homeobox Gene *HEX*

Mitsuru Inamura[1,2], Kenji Kawabata[2,3], Kazuo Takayama[1,2], Katsuhisa Tashiro[2], Fuminori Sakurai[2], Kazufumi Katayama[1,2], Masashi Toyoda[4], Hidenori Akutsu[4], Yoshitaka Miyagawa[5], Hajime Okita[5], Nobutaka Kiyokawa[5], Akihiro Umezawa[4], Takao Hayakawa[6,7], Miho K Furue[8,9] and Hiroyuki Mizuguchi[1,2]

[1]Department of Biochemistry and Molecular Biology, Graduate School of Pharmaceutical Sciences, Osaka University, Osaka, Japan; [2]Laboratory of Stem Cell Regulation, National Institute of Biomedical Innovation, Osaka, Japan; [3]Department of Biomedical Innovation, Graduate School of Pharmaceutical Science, Osaka University, Osaka, Japan; [4]Department of Reproductive Biology, National Institute for Child Health and Development, Tokyo, Japan; [5]Department of Developmental Biology and Pathology, National Institute for Child Health and Development, Tokyo, Japan; [6]Pharmaceutics and Medical Devices Agency, Tokyo, Japan; [7]Pharmaceutical Research and Technology Institute, Kinki University, Osaka, Japan; [8]JCRB Cell Bank/Laboratory of Cell Culture, Department of Disease Bioresource, National Institute of Biomedical Innovation, Osaka, Japan; [9]Laboratory of Cell Processing, Institute for Frontier Medical Sciences, Kyoto University, Kyoto, Japan

Human embryonic stem cells (ESCs) and induced pluripotent stem cells (iPSCs) have the potential to differentiate into all cell lineages, including hepatocytes, *in vitro*. Induced hepatocytes have a wide range of potential application in biomedical research, drug discovery, and the treatment of liver disease. However, the existing protocols for hepatic differentiation of PSCs are not very efficient. In this study, we developed an efficient method to induce hepatoblasts, which are progenitors of hepatocytes, from human ESCs and iPSCs by overexpression of the *HEX* gene, which is a homeotic gene and also essential for hepatic differentiation, using a HEX-expressing adenovirus (Ad) vector under serum/feeder cell-free chemically defined conditions. Ad-HEX-transduced cells expressed α-fetoprotein (AFP) at day 9 and then expressed albumin (ALB) at day 12. Furthermore, the Ad-HEX-transduced cells derived from human iPSCs also produced several cytochrome P450 (CYP) isozymes, and these P450 isozymes were capable of converting the substrates to metabolites and responding to the chemical stimulation. Our differentiation protocol using Ad vector-mediated transient HEX transduction under chemically defined conditions efficiently generates hepatoblasts from human ESCs and iPSCs. Thus, our methods would be useful for not only drug screening but also therapeutic applications.

Received 18 March 2010; accepted 13 October 2010; published online 23 November 2010. doi:10.1038/mt.2010.241

INTRODUCTION

Human embryonic stem cells (ESCs) and induced pluripotent stem cells (iPSCs) are able to replicate indefinitely and differentiate into most cell types of the body,[1–4] and thereby have the potential to provide an unlimited source of cells for a variety of applications.[5] Hepatocytes are useful cells for biomedical research, regenerative medicine, and drug discovery. They are particularly applicable to drug screenings, such as for the determination of metabolic and toxicological properties of drug compounds in *in vitro* models, because the liver is the main detoxification organ in the body.[6] For these applications, it is necessary to prepare a large number of functional hepatocytes from human ESCs and iPSCs. Many of the existing methods for cell differentiation of human ESCs and iPSCs into hepatocytes employ undefined, serum-containing medium and feeder cells.[7–9] Preparation of human ESC- and iPSC-derived hepatocytes for therapeutic applications and drug toxicity testing in humans should be done in nonxenogenic culture systems to avoid potential contamination with pathogens. Furthermore, the efficiency of the differentiation of the human ESCs and iPSCs into hepatocytes is not particularly high using these methods.[9–14]

In vertebrate development, the liver is derived from the primitive gut tube, which is formed by a flat sheet of cells called the definitive endoderm.[5,15] Shortly afterwards, the definitive endoderm is separated into endoderm derivatives containing the liver bud, the cells of which are referred to as hepatoblasts. The hepatoblasts have the potential to proliferate and differentiate into both hepatocytes and cholangiocytes. In the process of hepatic differentiation, the maturation is characterized by the expression of liver- and stage-specific genes. For example, α-fetoprotein (AFP) is an early hepatic marker, which is expressed in hepatoblasts in the liver bud until birth, and its expression is dramatically reduced after birth.[16] In contrast, albumin (ALB), which is the most abundant protein synthesized by hepatocytes, is initially expressed at lower levels in early fetal hepatocytes, but its expression level is increased as the hepatocytes mature, reaching a maximum in adult hepatocytes.[17] Furthermore, isoforms of cytochrome P450 (CYP) proteins also exhibit differential expression levels according to the developmental stages

Correspondence: *Hiroyuki Mizuguchi, Department of Biochemistry and Molecular Biology, Graduate School of Pharmaceutical Sciences, Osaka University, 1-6 Yamadaoka, Suita, Osaka 565-0871, Japan. E-mail: mizuguch@phs.osaka-u.ac.jp*

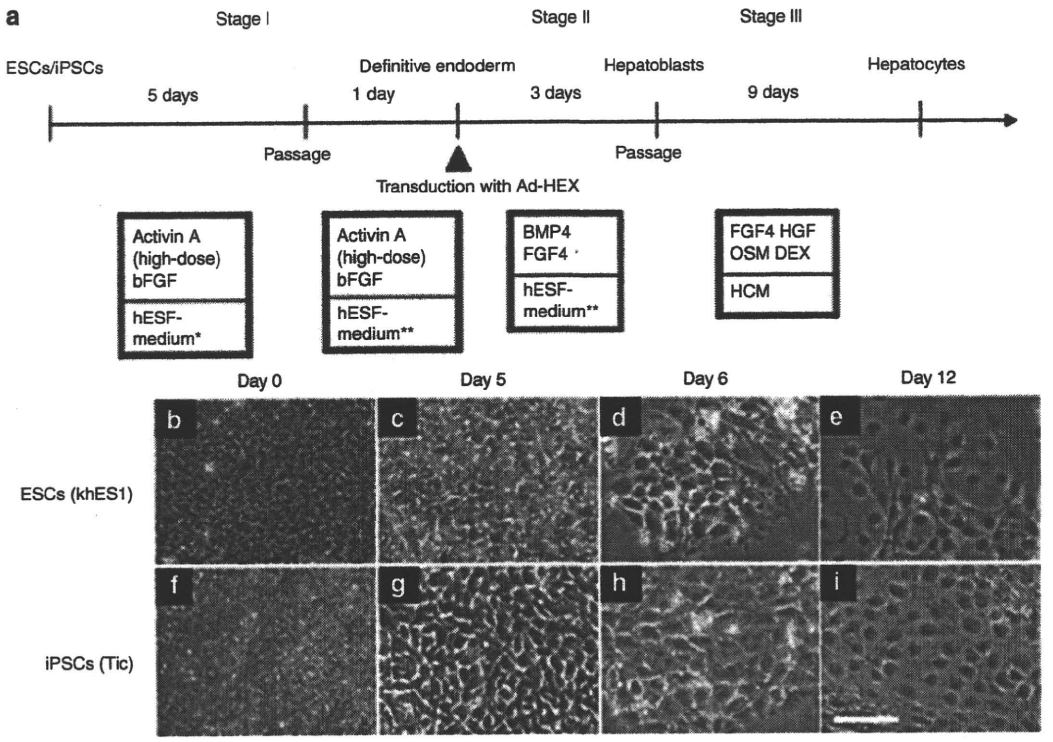

Figure 1 A strategy of differentiation of human embryonic stem cells (ESCs) and induced pluripotent stem cells (iPSCs) to hepatoblasts and hepatocytes. (a) Schematic representation illustrating the procedure for differentiation of human ESCs (khES1) and iPSCs (Tic) to hepatocytes. **(b–i)** Phase contrast microscopy showing sequential morphological changes (day 0–12) from **(b–e)** human ESCs (khES1) and **(f–i)** iPSCs (Tic) to hepatoblasts via the definitive endoderm. Bar = 50 µm. bFGF, basic fibroblast growth factor; BMP4, bone morphogenetic protein 4; DEX, dexamethasone; FGF4, fibroblast growth factor 4; HGF, hepatocyte growth factor; OSM, Oncostatin M; HCM, hepatocytes culture medium; *, hESF-GRO medium that was supplemented with 10 µg/ml human recombinant insulin, 5 µg/ml human apotransferrin, 10 µmol/l 2-mercaptoethanol, 10 µmol/l ethanolamine, 10 µmol/l sodium selenite, 0.5 mg/ml fatty acid free BSA; **, hESF-DIF medium that was supplemented with 10 µg/ml insulin, 5 µg/ml apotransferrin, 10 µmol/l 2-mercaptoethanol, 10 µmol/l ethanolamine, 10 µmol/l sodium selenite, 0.5 mg/ml BSA.

of the liver. Although most CYPs (including CYP3A4, CYP7A1, and CYP2D6) are only slightly expressed or not detected in the fetal liver tissue, the expression levels are dramatically increased after birth.[18]

For the development of hepatoblasts, numerous transcription factors are required, such as hematopoietically expressed homeobox (*HEX*), GATA-binding protein 6, prospero homeobox 1, and hepatocyte nuclear factor 4A.[15,19] Among them, *HEX* is suggested to function at the earliest stage of hepatic linage.[20] HEX is first expressed in the definitive endoderm and becomes restricted to the future hepatoblasts. Targeted deletion of the *HEX* gene in the mouse results in embryonic lethality and a dramatic loss of the fetal liver parenchyma.[19,21,22] The hepatic genes, including *ALB*, prospero homeobox1, and hepatocyte nuclear factor 4A, are transiently expressed in the definitive endoderm of *HEX*-null embryos, and further morphogenesis of the hepatoblasts does not occur.[23] In general, then, *HEX* is essential for the definitive endoderm to adopt a hepatic cell fate.

Adenovirus (Ad) vectors are one of the most efficient gene delivery vehicles and have been widely used in both experimental studies and clinical trials.[24] Ad vectors are attractive vehicles for gene transfer because they are easily constructed, can be prepared in high titers, and provide high transduction efficiency in both dividing and nondividing cells. We have developed efficient methods for Ad vector-mediated transient transduction into mouse ESCs and iPSCs.[25,26] We have also showed that the differentiations of mouse ESCs and iPSCs into adipocytes and osteoblasts were dramatically promoted by Ad vector-mediated peroxisome proliferator activated receptor γ and runt related transcription factor 2 transduction, respectively.[25,26]

In this study, we hypothesized that transient *HEX* transduction could efficiently induce hepatoblasts from human ESCs and iPSCs. A previous study demonstrated that *HEX* regulates the differentiation of hemangioblasts and endothelial cells from mouse ESCs,[27] whereas the role of *HEX* in the differentiation of hepatoblasts from human ESCs and iPSCs remains unknown. We found that differentiation of hepatoblasts from the human ESC- and iPSC-derived definitive endoderms, but not from undifferentiated human ESCs and iPSCs, could be facilitated by Ad vector-mediated transient transduction of a *HEX* gene. Furthermore, the Ad-HEX-transduced cells that were derived from human iPSCs were able to differentiate into functional hepatocytes *in vitro*. All the processes for cellular differentiation were performed under serum/feeder cell- free chemically defined conditions. Our culture systems and differentiation method based on Ad vector-mediated transient transduction under chemically defined conditions would provide a platform for drug screening as well as safe therapies.

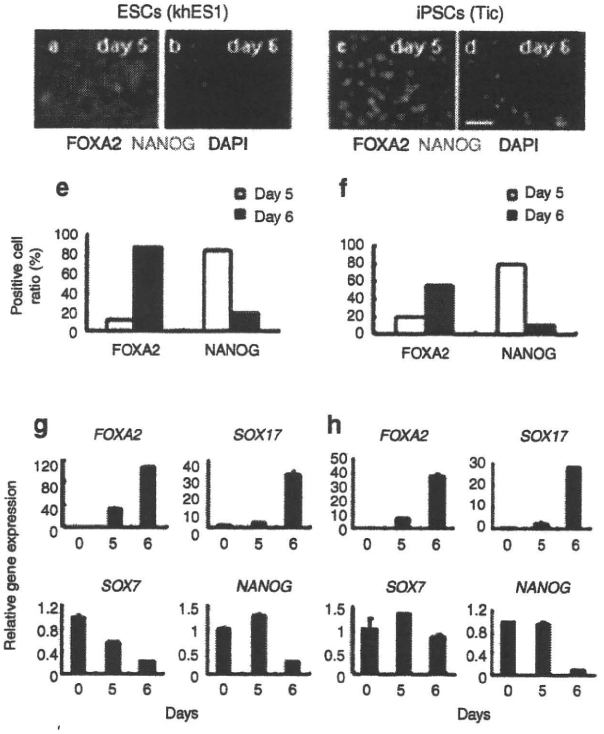

Figure 2 Characterization of the human ESC (khES1)- and iPSC (Tic) derived definitive endoderms. (**a–d**) The immunofluorescent staining of the human ESC (khES1)- and iPSC (Tic) derived differentiated cells before (**a** and **c**; day 5) and after passaging (**b** and **d**; day 6). The cells were immunostained with antibodies against FOXA2 and NANOG. Nuclei were stained with DAPI. (**e,f**) Semiquantitative analysis of the immunofluorescent staining in **a–d**. Data are presented as the mean of immunopositive cells counted in eight independent fields. (**g,h**) Real-time RT-PCR analysis of the level of definitive endoderm (*FOXA2* and *SOX17*), pluripotent (*NANOG*), and extra-embryonic endoderm (*SOX7*) gene expression at day 5 and 6. At day 5, the cells were passaged. Therefore, the data at day 5 and 6 show the levels of gene expression before (at day 5) or after the passage (at day 6). Data are presented as the mean ± SD from triplicate experiments. The graphs represent the relative gene expression level when the level of undifferentiated cells at day 0 was taken as 1. Bar = 50 μm. ESC, embryonic stem cells; iPSC, induced pluripotent stem cells.

RESULTS

Differentiation of human ESC- and iPSC-derived definitive endoderms

Our three-step differentiation protocol is illustrated in Figure 1a. After treatment with 50 ng/ml of Activin A (high-dose) and basic fibroblast growth factor (bFGF) for 5 days on a laminin-coated plate, morphologically, the human ESCs and iPSCs were gradually transformed from typical, defined, tight human ESC, and iPSC colonies (day 0) into less dense, flatter cells containing prominent nuclei (day 5), even though the majority of the cells had a morphology resembling that of undifferentiated cells (**Figure 1b,c,f,g**). FACS analysis showed that ~46% of human iPSC-derived differentiated cells expressed CXCR4 (expressed in the definitive endoderm but not the primitive endoderm) (**Supplementary Figure S1a**). Human ESC- and iPSC-derived differentiated cells were immunostained with the definitive endoderm marker, FOXA2 (**Figure 2a,c**). However, the majority of the cells expressed the pluripotent marker NANOG, indicating that undifferentiated cells remain in the induced cultures at day 5. After the cells were passaged with trypsin-EDTA and seeded on a laminin-coated plate a second time, the resultant cells were found to be more homogeneous and flatter at day 6 (**Figure 1d,h**). Semiquantitative analysis by counting immunopositive cells revealed that the number of FOXA2-positive cells was increased and, in turn, the number of NANOG-positive cells was decreased at day 6 after passaging (**Figure 2e,f**). Real-time reverse transcriptase (RT)-PCR analysis showed that the definitive endoderm markers *FOXA2* and *SOX17* mRNA were upregulated, whereas the pluripotent marker *NANOG* mRNA was downregulated at day 6 (**Figure 2g,h**). These results were consistent with the immunofluorescence results (**Figure 2a–d**). The expression levels of the mesoderm marker *FLK1* mRNA and ectoderm marker *PAX6* mRNA were downregulated or unchanged at day 6 (**Supplementary Figure S1b–e**). Importantly, the expression of *SOX7* mRNA (expressed in the extra-embryonic endoderm but not the definitive endoderm) was downregulated (**Figure 2g,h**). These results indicate that the definitive endoderm is induced or selected from human ESCs and iPSCs after passaging. We obtained the same results using another human iPSC line (**Supplementary Figure S2a–d**).

HEX induces hepatoblasts from the human ESC- and iPSC-derived definitive endoderms

To investigate whether forced expression of transcription factors could promote hepatic differentiation, the human ESC- and iPSC-derived definitive endoderms were transduced with Ad vectors. We used a fiber-modified Ad vector containing the elongation factor-1α promoter and a stretch of lysine residue (K7) peptides in the C-terminal region of the fiber knob to examine the transduction efficiency in the human ESC- and iPSC-derived definitive endoderms. The elongation factor-1α promoter was found to be highly active in human ESCs.[28] The K7 peptide targets heparan sulfates on the cellular surface, and the fiber-modified Ad vector containing K7 peptides was shown to be efficient for transduction into many kinds of cells.[29,30] The human ESC- and iPSC-derived definitive endoderms were transduced with a LacZ-expressing Ad vector (Ad-LacZ) at 3,000 vector particle/cell. X-Gal staining showed that the Ad-LacZ-transduced human ESC- and iPSC-derived definitive endoderms successfully expressed LacZ (**Figure 3**). Nearly 100% of the cells transduced with Ad-LacZ were strongly X-gal positive. The transduction efficiency in the human ESC- and iPSC-derived definitive endoderms transduced with the conventional Ad vector containing the wild-type capsid at 3,000 vector particle/cell was ~80% and X-gal staining was much weaker than that in the cells transduced with fiber-modified Ad vectors (**Supplementary Figure S6**).

Next, the human ESC- and iPSC-derived definitive endoderms were transduced with a HEX-expressing fiber-modified Ad vector (Ad-HEX). Although HEX is known to be a transcription factor that is essential for liver development, it remains unclear what the effect of transient *HEX* overexpression is on differentiation from human ESCs and iPSCs or their derivatives *in vitro*. We confirmed the overexpression of *HEX* in the human ESC- and iPSC-derived definitive endoderms transduced with Ad-HEX (**Supplementary Figure S3a–f**). Gene expression analysis revealed the upregulation of *AFP* mRNA, which was expressed by hepatoblasts or early hepatocytes, in Ad-HEX-transduced cells as

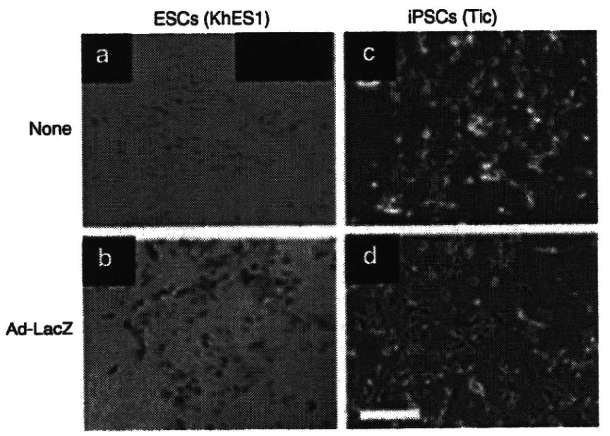

Figure 3 Efficient transgene expression in the human ESC (khES1)- and iPSC (Tic) derived definitive endoderms by using a fiber-modified Ad vector containing the EF-1α promoter. (a,b) Human ESC (khES1)-derived and **(c,d)** iPSC (Tic) derived definitive endoderms were transduced with 3,000 VP/cell of Ad-LacZ for 1.5 hours. The next day after transduction, X-gal staining was performed as described in the Materials and Methods section. Similar results were obtained in two independent experiments. Scale = 50 μm. Ad, adenovirus; EF-1α, elongation factor-1α; ESC, embryonic stem cells; iPSC, induced pluripotent stem cells; LacZ, Ad-LacZ-transduced cells; None, nontransduced cells.

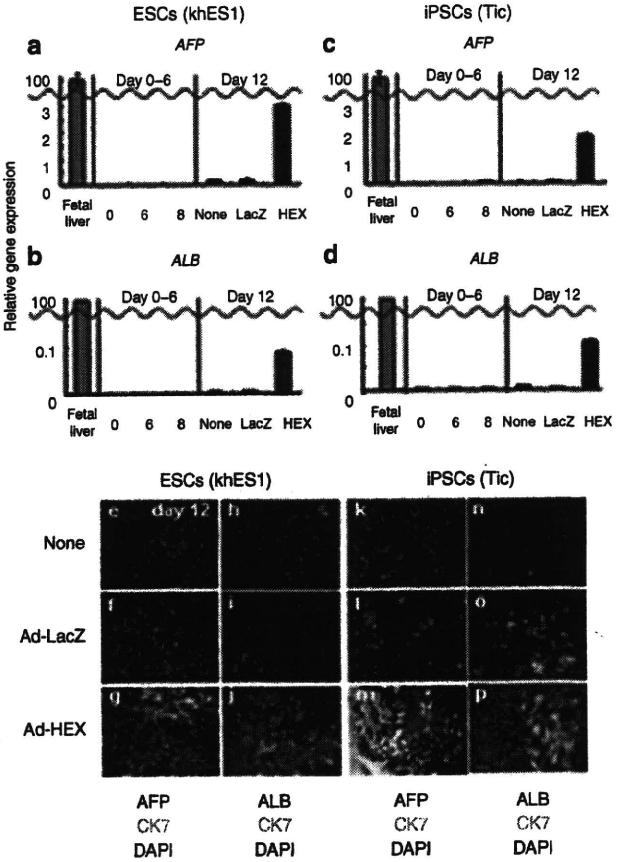

Figure 4 Efficient hepatoblast differentiation from the human ESC (khES1)- and iPSC (Tic) derived definitive endoderms by transduction of the *HEX* gene. (a–d) Real-time RT-PCR analysis of the level of **(a,c)** *AFP* and **(b,d)** *ALB* expression in nontransduced cells, Ad-LacZ-transduced cells, and Ad-HEX-transduced cells, all of which were induced from the human ESC (khES1)- and iPSC (Tic) derived definitive endoderms (day 0, 5, 6, and 12). The cells were transduced with Ad-LacZ or Ad-HEX at day 6 as described in **Figure 1a**. The data at day 6 was obtained before the transduction with Ad-HEX. The graphs represent the relative gene expression levels when the level in the fetal liver was taken as 100. **(e–p)** Immunocytochemistry of AFP, ALB, and CK7 expression in nontransduced cells (**e,h,k,** and **n**), Ad-LacZ-transduced cells (**f,i,l,** and **o**), and Ad-HEX-transduced cells (**g,j,m,** and **p**) at day 12, all of which were induced from the human ESC (khES1)- and iPSC (Tic) derived definitive endoderms. Nuclei were stained with DAPI. Bar = 50 μm. Ad, adenovirus; AFP, α-fetoprotein; ALB, albumin; CK7, cytokeratin 7; HEX, Ad-HEX-transduced cells; ESC, embryonic stem cells; iPSC, induced pluripotent stem cell; LacZ, Ad-LacZ-transduced cells; None, nontransduced cells.

compared with nontransduced cells or Ad-LacZ-transduced cells (**Figure 4a,c**). Expression of *ALB* mRNA, which is the most abundant protein in liver, was also observed in Ad-HEX-transduced cells (**Figure 4b,d**).

During liver development, both hepatocytes and cholangiocytes were differentiated from the hepatoblasts. We examined the protein expression of AFP, ALB, and the cholangiocyte marker cytokeratin 7 (CK7) in Ad-HEX-transduced cells by immunostaining (**Figure 4e–p**). The AFP-positive populations were detected in Ad-HEX-transduced cells (**Figure 4g,m**). ALB-positive cells were also detected, although the detection efficiency was very low (**Figure 4j,p**). CK7-positive cells were observed among the Ad-HEX-transduced cells, and all CK7-positive cells were found near the AFP- and ALB-positive cells, suggesting that hepatoblasts are generated by the transient overexpression of a *HEX* gene. Semiquantitative RT-PCR analysis showed that the expression levels of the liver-enriched transcription factors hepatocyte nuclear factor 1A, hepatocyte nuclear factor 1B, hepatocyte nuclear factor 4A, and hepatocyte nuclear factor 6 mRNA were upregulated in Ad-HEX-transduced cells (**Supplementary Figure S4a,b**). The expressions of CCAAT/enhancer binding protein α and prospero homeobox 1 mRNA, two transcription factors known to play a pivotal role in the establishment of the hepatoblasts, were also induced in Ad-HEX-transduced cells (**Supplementary Figure S4a, b**). Taken together, these findings indicate that *HEX* enhances the specification of hepatoblasts from the human ESC- and iPSC-derived definitive endoderms. Similar results were obtained with another human iPSC line (**Supplementary Figure S2e–g**).

Time course of differentiation of the definitive endoderm to hepatoblasts

Next, we examined the time course of AFP and CK7 expression during differentiation of human iPSCs to hepatoblasts in Ad-HEX-transduced cells and nontransduced cells. At day 7 (the day after transduction), the expression of AFP was not detectable in Ad-HEX-transduced or nontransduced cells (**Supplementary Figure S5a,d**). At day 8–9, morphological changes to hepatocyte-like cells were observed in Ad-HEX-transduced cells (**Supplementary Figure S5h,i**). We also observed homogeneous AFP-positive cells at day 9 (**Supplementary Figure S5e**). At day 10, CK7-positive cells appeared, indicating that hepatoblasts started to differentiate into hepatocytes and cholangiocytes at day 9–10 (**Supplementary Figure S5f**). At day 12, ALB-positive cells appeared, indicating that hepatocytes were differentiated from Ad-HEX-transduced cells (**Figure 4p**). These results showed that *HEX* induces the hepatoblasts from the

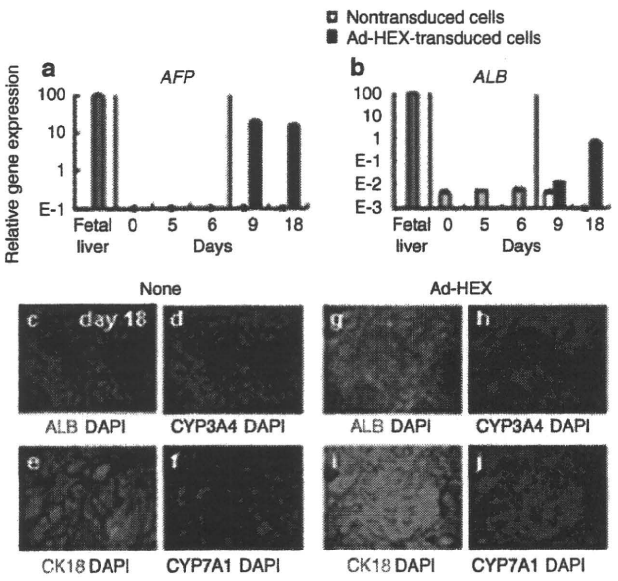

Figure 5 Efficient differentiation of Ad-HEX-transduced hepatoblasts into hepatocytes. (**a**,**b**) Real-time RT-PCR analysis of (**a**) *AFP* and (**b**) *ALB* expression in nontransduced cells and Ad-HEX-transduced cells, both of which were induced from the human iPSC (Tic) derived definitive endoderm (day 0, 5, 6, and 12). The cells were transduced with Ad-HEX at day 6 as described in **Figure 1a**. The data at day 6 were obtained before the transduction with Ad-HEX. The graphs represent the relative gene expression level when the level in the fetal liver was taken as 100. (**c–j**) Immunocytochemistry of ALB, CYP3A4, CYP7A1, and CK18 expression in (**c–f**) nontransduced cells and (**g–j**) Ad-HEX-transduced cells, all of which were induced from the human iPSC (Tic) derived definitive endoderm at day 18. Nuclei were stained with DAPI. Bar = 50 μm. Ad, adenovirus; AFP, α-fetoprotein; ALB, albumin; CK18, cytokeratin 18; ESC, embryonic stem cells; HEX, Ad-HEX-transduced cells; iPSC, induced pluripotent stem cell; None, nontransduced cells; RT-PCR, reverse transcriptase-PCR.

definitive endoderm, and the Ad-HEX-transduced cells could differentiate into both hepatocytes and cholangiocytes.

Directed hepatic differentiation from hepatoblasts

With the protocol described above, heterogeneous populations containing CK7-positive cholangiocytes were observed at day 12 (**Figure 4p**). To promote the differentiation of hepatoblasts to hepatocytes, the human iPSC-derived differentiated cells at day 9 (**Supplementary Figure S5e**) were dislodged with trypsin-EDTA and plated on collagen I-coated dishes as previously reported.[11] After 8–11 days in culture with medium containing FGF4, HGF, OSM, and DEX, the Ad-HEX-transduced cells became more flattened (**Supplementary Figure S5m**), whereas the nontransduced cells became fibroblast-like cells (**Supplementary Figure S5i**). Gene expression analysis showed the upregulation of *ALB* mRNA in Ad-HEX-transduced cells under this culture condition, whereas the expression of *ALB* mRNA was reduced in the nontransduced cells at day 18 (**Figure 5b**). Immunostaining showed that only a small percentage of Ad-HEX-transduced cells expressed ALB at day 12 (**Figure 4p**), whereas most of the Ad-HEX-transduced cells were ALB-positive at day 18 (**Figure 5g**). Most of the Ad-HEX-transduced cells also expressed CYP3A4 at day 18 (**Figure 5h**). More importantly, in the Ad-HEX-transduced cells, CYP7A1 and cytokeratin 18 were detected and these proteins are known

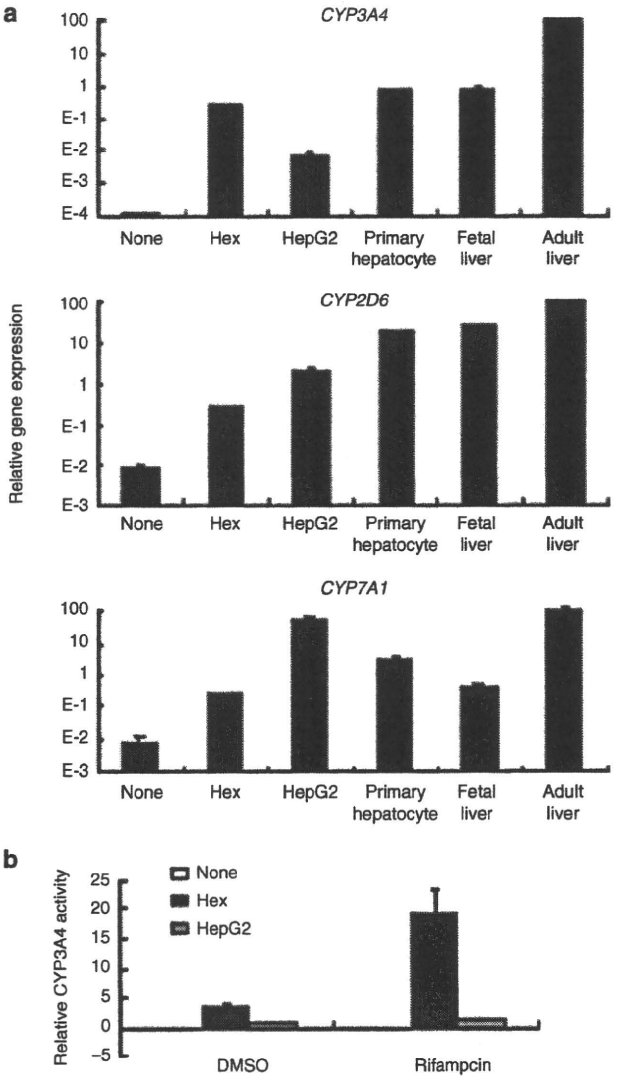

Figure 6 Cytochrome P450 isozymes in human iPSC (Tic) derived hepatocytes. (**a**) Real-time RT-PCR analysis of *CYP3A4*, *CYP7A1*, and *CYP2D6* expression in iPSC (Tic) derived nontransduced cells, Ad-HEX-transduced cells, and fetal and adult liver tissues. (**b**) Induction of CYP3A4 by rifampicin in human iPSC (Tic) derived nontransduced cells, Ad-HEX-transduced cells, the HepG2 cell line and primary human hepatocytes, which were cultured 48 hours after plating the cells. Data are presented as the mean ± SD from triplicate experiments. The graphs represent the relative gene expression level when the level in the adult liver was taken as 100. AFP, α-fetoprotein; ALB, albumin; DMSO, dimethyl sulfoxide; ESC, embryonic stem cells; HEX, Ad-HEX-transduced cells; iPSC, induced pluripotent stem cell; LacZ, Ad-LacZ-transduced cells; None, nontransduced cells.

to be detected in hepatocytes but not in extra-embryonic cells[31,32] (**Figure 5i,j**). Quantitative analysis showed that ~84, 80, 88, and 92% of Ad-HEX-transduced cells expressed ALB, CYP3A4, CYP7A1, and cytokeratin 18, respectively. These results indicate that Ad-HEX-transduced cells could differentiate to hepatic cells. However, the expression level of *ALB* mRNA in Ad-HEX-transduced cells was lower than that in fetal liver tissue and in turn, the expression of *AFP* mRNA was maintained (**Figure 5a**). Therefore, Ad-HEX-transduced cells are committed to the hepatic linage, but are not yet mature hepatocytes.